UNIVERSITY OF CALIFORNIA,

IRVINE

Developing a Cellular DNA-Encoded Library Screening Platform

THESIS

submitted in partial satisfaction of the requirements
for the degree of

MASTER OF SCIENCE

in Pharmacological Sciences

by

Jessica Jenna Su

Thesis Committee:
Professor Brian M. Paegel, Committee Chair
Professor David L. Mobley, Departmental Vice Chair
Professor Robert C. Spitale, Founding Associate Dean of Research

2021

Table of Contents

List of Figures

Acknowledgements

I would like to thank my thesis advisor, Dr. Brian Paegel, for his mentorship and guidance throughout my graduate studies. I would also like to thank Jeffrey Lam, who worked on other aspects of this project, and Huda Barhoosh, Patrick Fitzgerald, Anjali Dixit, Amber Hackler, and Val Cavett of the Paegel lab for their support in the lab. I must also thank Allan Argelagos, Ana Caldaruse, Shaan Sheikh, Enya Li, Camryn Rambo, Dena Amiri, and Dr. Anthony Mascola for the constant emotional support that got me through the stresses of graduate school. Finally, I need to thank Kyle Pacheco for being my rock, giving me a home to bring my joys and trials, and sharing life with me through it all.

Abstract

Developing a Cellular DNA-Encoded Library Screening Platform

by

Jessica Jenna Su

Master of Science in Pharmacological Sciences

University of California, Irvine 2021

Professor Brian M. Paegel, Chair

DNA-encoded library (DEL) technology is a powerful next-generation drug discovery engine. DELs permit the design and synthesis of large, customized molecular libraries, which can be mined for new ligands by affinity selection. More advanced screening technology has emerged that enables direct activity-based DEL screening, but to date, this is limited to biochemical activity assays. Cellular assays, which are vital for discovering physiologically relevant novel chemical matter, are still incompatible with DEL. Here, I describe a prospective workflow that renders DEL compatible with cellular activity assays. Cells are grown directly on DEL beads, which effectively serve as microcarriers. The cells are engineered to secrete a reporter upon stimulation with an agonist, which is liberated from the DEL bead via photocleavage. The microcarrier is functionalized with affinity tag ligands, which capture the affinity-tagged secreted reporter. Toward this goal, I have engineered cell lines that secrete HaloTag-labeled fluorescent protein reporters, shown that reporter cell lines can grow and signal on microcarriers, and explored photocleavage conditions that permit

efficient photochemistry while preserving cell viability. Additional studies were conducted to identify appropriate positive control ligands of a model cellular target, STING (stimulator of interferon genes). This thesis lays the groundwork for a DEL-compatible cellular assay paradigm that can be adapted to an array of cell-based assay strategies.

Introduction: Laying the Groundwork for Cellular DNA-Encoded Library-Based Screening Platforms

Efficient screening of large compound libraries is critical for early-stage drug discovery. High-throughput screening (HTS), the conventional method for discovering new drug leads, is an automated platform[1] that allows screening of ~10^6 compounds – each stored in a well of a microtiter plate – against diverse assays of bioactivity, from purified proteins[2,3,4] to whole cells[5,6,7] and tissues[8,9,10]. DNA-encoded libraries (DELs), which result from encoded combinatorial synthesis, are a widely implemented and complementary source of chemical diversity. DELs contain millions of unique small molecules with a DNA sequence encoding the molecule's synthetic makeup[11]. DELs are analyzed strictly by affinity selection of library members that bind a protein target of interest. I will discuss the successes and limitations of DEL affinity selection, the emergence of activity-based DEL technology, and progress toward adapting DEL to cell-based assays.

Hit finding using conventional DEL technology occurs via affinity selection. In an affinity selection, the DEL is incubated with a protein target, bound DEL members are isolated, and the DNA encoding tags of the bound fraction are sequenced and decoded to ascertain the novel ligand structures. Affinity selection can evaluate billions of compounds in a single binding assay. While the technique has led to the discovery of ligands for various target classes[12] such as kinases[13,14,15,16,17], hydrolases[18,19], aminotransferases[20], cell-surface receptors[21,22,23,24,25], and protein-protein interactions[26,27,28], the approach is not generally amenable to ion channels, transcription

factors, protein complexes, and signal transduction pathways. The protein of interest generally must fold and express well, exhibit minimal intrinsic disorder, and not promiscuously bind nucleic acids (among other constraints)[29].

Our lab has pioneered an activity-based DEL screening platform, which opens the door to investigating complex targets outside the scope of affinity selection. Using a droplet-based microfluidic circuit, Cochrane et al. screened solid-phase DELs for inhibitors of the phosphodiesterase autotaxin[11]. The device encapsulates DEL beads into microfluidic droplets of activity assay reagent, photocleaves the DEL member from its bead, incubates the assay, and reads the assay endpoint in each droplet, sorting for collection those droplets with an appropriately high (or low) assay signal. The approach allows one to identify active DEL members directly using standard biochemical HTS assay technology: here, an enzyme turning over a fluorogenic substrate to yield a fluorescent product **(Fig 1)**.

Cell-based assays, which are also of interest, generally follow similar assay development protocols. Cells are seeded onto well plates, treated with a compound, and then analyzed[30] **(Fig 2A)**. If they secrete a reporter, the media is collected, incubated with a substrate, and enzymatic readout is measured with a fluorescence microplate reader[30] **(Fig 2B)**. In a cytotoxicity assay, cells are stained for viability, which is quantified by flow cytometry[31]. Advanced imaging technology such as imaging cytometry can produce phenotypic readouts for single-cell analysis of cell morphology[32].

We have chosen to work with the cyclic GAMP synthase – stimulator of

Figure 1. Activity-based DEL circuit

A schematic of activity-based DNA-encoded library (DEL) screening for autotaxin inhibitors. Droplets encapsulate autotaxin, DEL members, and fluorophore (F) and quencher (Q) bound by a phosphodiester bond. Fluorophore photon emission is neutralized by the proximate quencher molecule. Autotaxin cleaves the phosphodiester bond between fluorophore and quencher to yield fluorescent fluorophore photon emission, turning the droplets green for sorting. “Hit” DEL members inhibit autotaxin activity, yielding dark droplets that can be sorted. Adapted from Cochrane et al. *ACS Combinatorial Science* (2019).

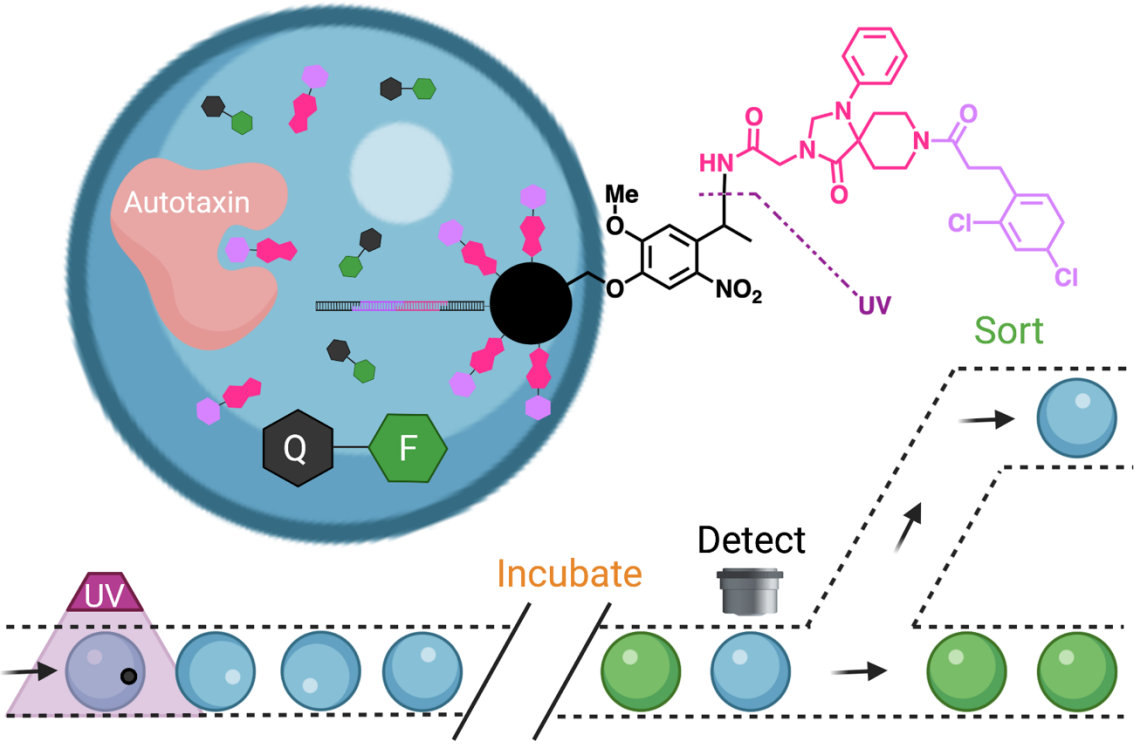

Created with Biorender.com

Figure 2. General cell-based assay schematic

A general schematic of a cell-based assay. **A** Cells are grown in a 24-well plate and treated with an agonist. **B** Cells secrete enzyme into the media, which is collected for assaying. **C** Cell-secreted enzyme and substrate are added to a 384-well plate, and the fluorescence signal from the enzymatic reaction converting fluorescein diphosphate to fluorescein is quantified by a fluorescence microplate reader.

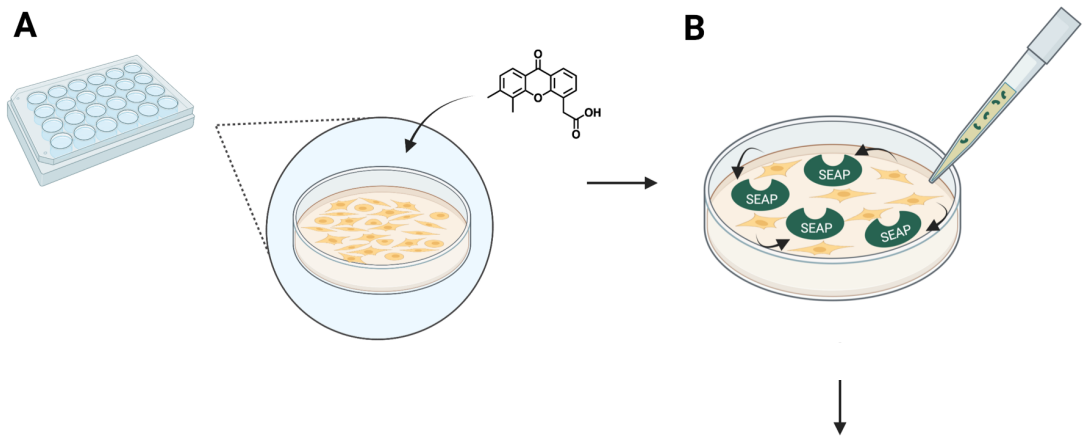

Created with BioRender.com

C

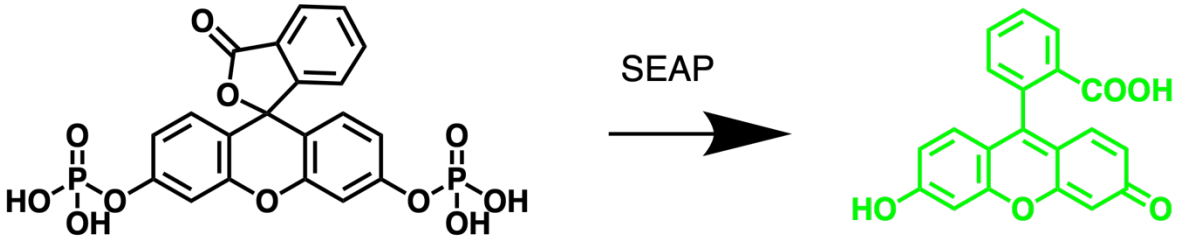

interferon genes (cGAS-STING) pathway as a model system for technology development. The cGAS-STING pathway is a component of the innate immune response, which detects pathogen activity and other signs of cellular stress[33]. cGAS-STING also an emerging oncology target because improper signaling can lead to cancer progression and metastasis[34]. cGAS is the primary sensor of the pathway. It binds cytosolic dsDNA and becomes activated, catalyzing the coupling of ATP and GTP to form cGAMP **(Fig 3)**. cGAMP then binds to STING, which, as it trafficks from the endoplasmic reticulum to the Golgi apparatus, activates the kinase TBK1 to phosphorylate IRF3 and the kinase IKK to phosphorylate IkB. Phospho-IKK releases NF-kB when degraded by the ubiquitin-proteasome pathway[33]. STING activation ultimately results in expression of type I interferons and proinflammatory cytokines. In a commercial STING signaling reporter cell line, phospho-IRF3 leads to the production of the secreted embryonic alkaline phosphatase (SEAP) reporter, and NF-kB drives expression of a luciferase reporter.

Cell-based assays are an important tool in the HTS-based early discovery tool box, but they are not amenable to microfluidic DEL screening. Most cell lines are adherent and will not grow in droplets because they are anchorage-dependent[35]. Cell viability during long incubations in droplets is challenging as well since agitation is required for adequate gas exchange[36]. The straightforward approach of forming droplets with DEL beads and cells using water-in-oil flow focusing droplet generation will result in empty droplets, droplets with multiple cells or DEL beads, and no method for ensuring that negative control cells are in every droplet. We need an approach that

Figure 3. cGAS-STING pathway

The commercial hSTING A162 and hSTING R232 HEK293T cell lines utilize the cGAS-STING pathway of cytosolic DNA sensing. cGAS is activated by cytosolic double-stranded DNA from damaged mitochondria, dead cells, bacteria, and viruses, and synthesizes cGAMP, the endogenous ligand for STING, from ATP and GTP. In the engineered construct, agonists bind to STING, leading to NF-kB and IRF3 phosphorylation. A SEAP reporter gene is inserted downstream of the 5X-ISRE transcription factor binding site, and phospho IRF3 produces SEAP expression. Adapted from Chen et al. *Nature Immunology* (2016).

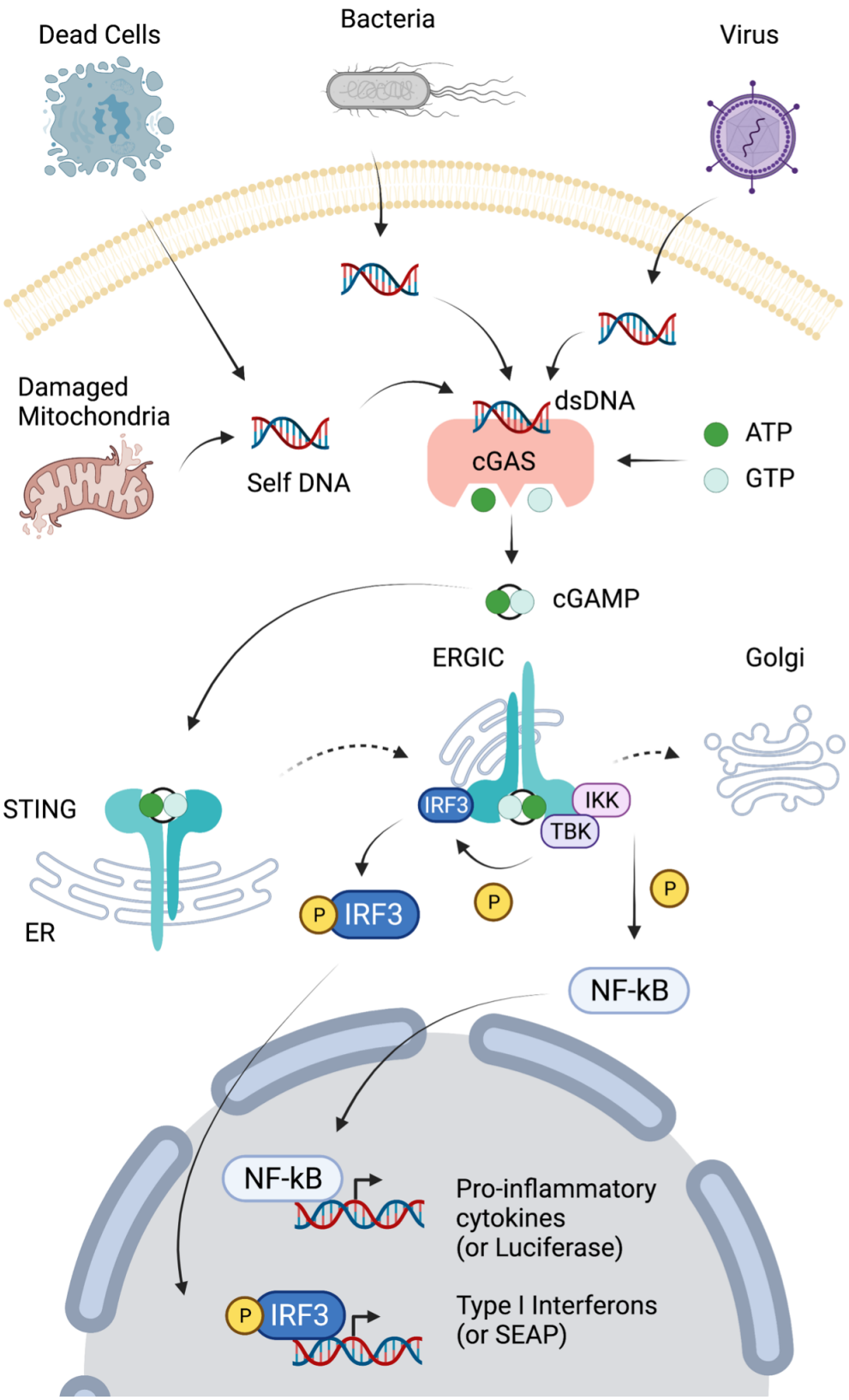

Created with BioRender.com

controls for the inherently higher variance of cell-based assays[37] and is compatible with adherent cell growth.

Microcarriers are a method to transform adherent cell culture into suspension culture. Microcarriers are microbeads that are slightly denser than water to support cell attachment and growth[38]. The high surface area to volume ratio of microcarriers allows high cell density in culture required by medical applications such as cell therapy, tissue engineering, and protein production[38]. Microcarrier technology also allows for 3D cell culture with adhesion, proliferation, and interactions mimicking the in vivo microenvironment[39]. The applications for microcarriers in cell culture are vast, and we propose here to expand this form of tissue culture to DEL screening.

To incorporate cell-based assays, our proposed workflow uses DEL beads as tissue culture microcarriers. We synthesized DEL compounds on photocleavable linkers **(Fig 4A)**, and transformed the DEL bead into a substrate that promotes cell adhesion and growth in tissue culture. Compounds are photocleaved with UV irradiation, resulting in proximity-driven stimulation of cell signaling. Hit compounds and positive control agonists induce STING signaling and SEAP reporter secretion, which are quantified with fluorescein diphosphate substrate to produce fluorescein product **(Fig 4B)**. Microcarrier beads are functionalized to capture affinity-tagged fluorescent product, resulting in labeling of the microcarrier **(Fig 4C)**. This approach solves many of the issues that arise with introducing cells to droplet-based DEL screening.

Figure 4. Proposed cellular DEL screening workflow

Cellular assay workflow for DEL screening using DEL beads as tissue culture microcarriers. **A** The positive control agonist, and eventually every compound in the library, is attached to a photocleavable linker on a solid phase resin. Each compound will also have a unique DNA tag. **B** Photocleavable compound release results in proximity-driven cell signaling. Cells are grown on hydrogel microcarriers encompassing the DEL bead. UV irradiation liberates the agonist, which induces cell signaling. Our commercial cell line expresses secreted embryonic alkaline phosphatase (SEAP), which will react with the substrate fluorescein diphosphate (FDP) to generate fluorescein dye (FAM). **C** Our workflow involves seeding cells onto hydrogel microcarriers, liberating DEL bead compounds with UV irradiation, capturing cellular signal with functionalized microcarriers, and sorting “hit” microcarriers by FACS.

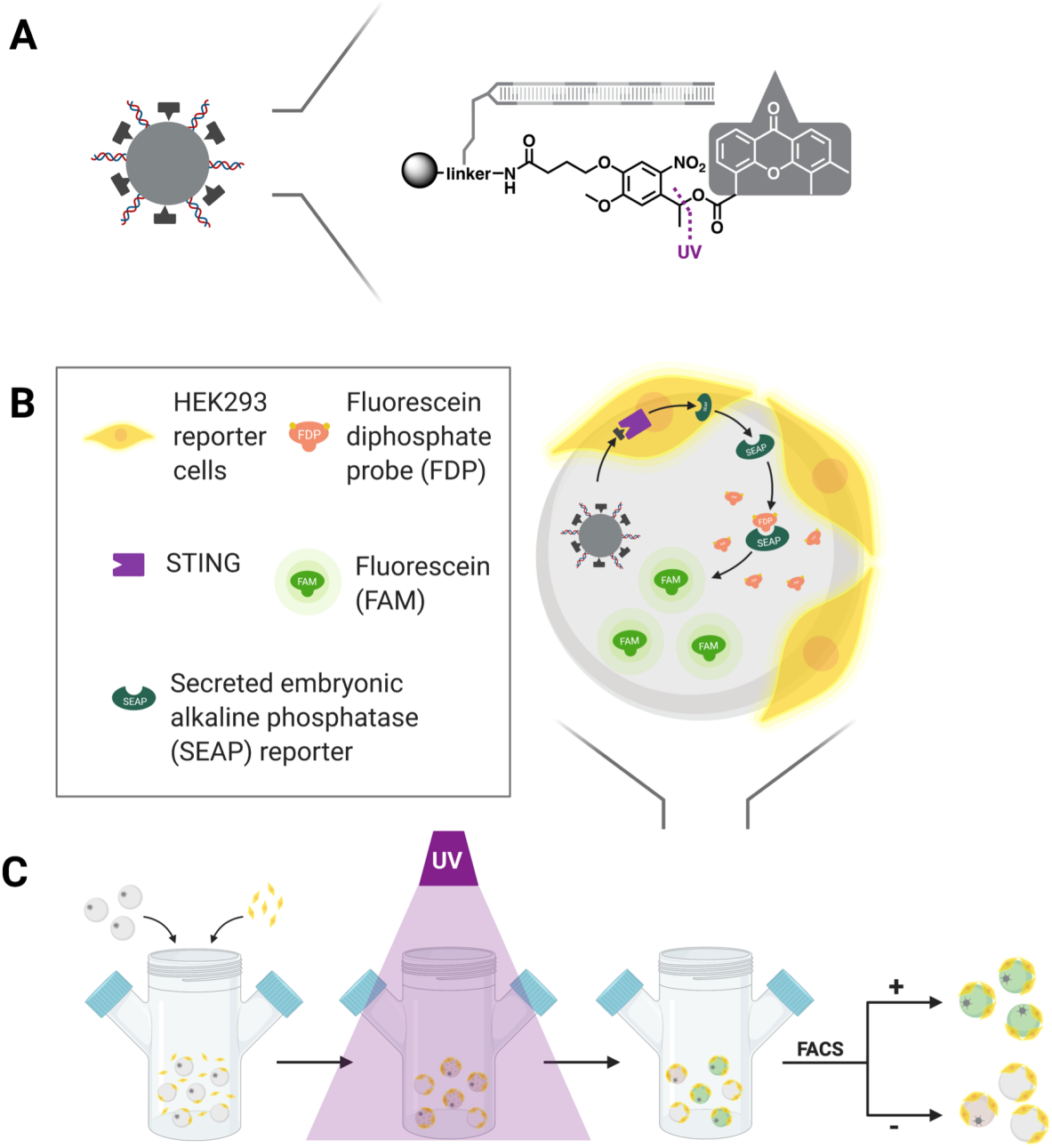

Created with BioRender.com

Demonstrating Cell Viability and Signaling on Commercial Microcarriers

Microcarrier culture is essential for cellular DEL screening assays. Adherent cells are averse to suspension growth in droplets due to the cytotoxicity of detergents and difficulty facilitating nutrient exchange. A solid surface for cell adhesion and proliferation is necessary. As a proof-of-concept, we began cell culture with commercial Cytodex I dextran microcarriers before proceeding to customized microcarriers that are amenable to use with DELs. After conditions were optimized for robust, even seeding, we demonstrated viability and detectable signaling from cells grown on Cytodex I microcarriers. These data established a foundation to build the cellular DEL screening platform.

We sought to find appropriate seeding conditions for even growth on microcarriers. We initially seeded HEK293 cells on Cytodex I microcarriers and used micro stir bars in 24-well plates to agitate the microcarriers and media both continuously (20 rpm) and intermittently (5 min on, 5 min off, 20 rpm), which yielded less than 50% seeding on microcarriers. After seeding cells onto microcarriers and leaving them overnight without agitation, we saw even cell seeding on 95% of microcarriers in each well. HEK293 cells grew to confluence on commercial Cytodex 1 microcarriers (**Fig 5**). With seeding conditions optimized, we moved forward with demonstrating cell viability.

We qualitatively and quantitatively showed that cells grown on Cytodex I microcarriers are viable. Cell viability was measured using live cell stain, cells were imaged with fluorescence microscopy, and live and dead cell stains were used in conjunction with flow cytometry analysis. Cells on Cytodex 1 microcarriers stained with

Figure 5. HEK293 cells on commercial microcarriers

HEK293 reporter cells adhere to and grow on commercial Cytodex 1 control microcarriers. Ideal conditions for robust, even seeding in a well plate are static rather than stirred with micro stir bars.

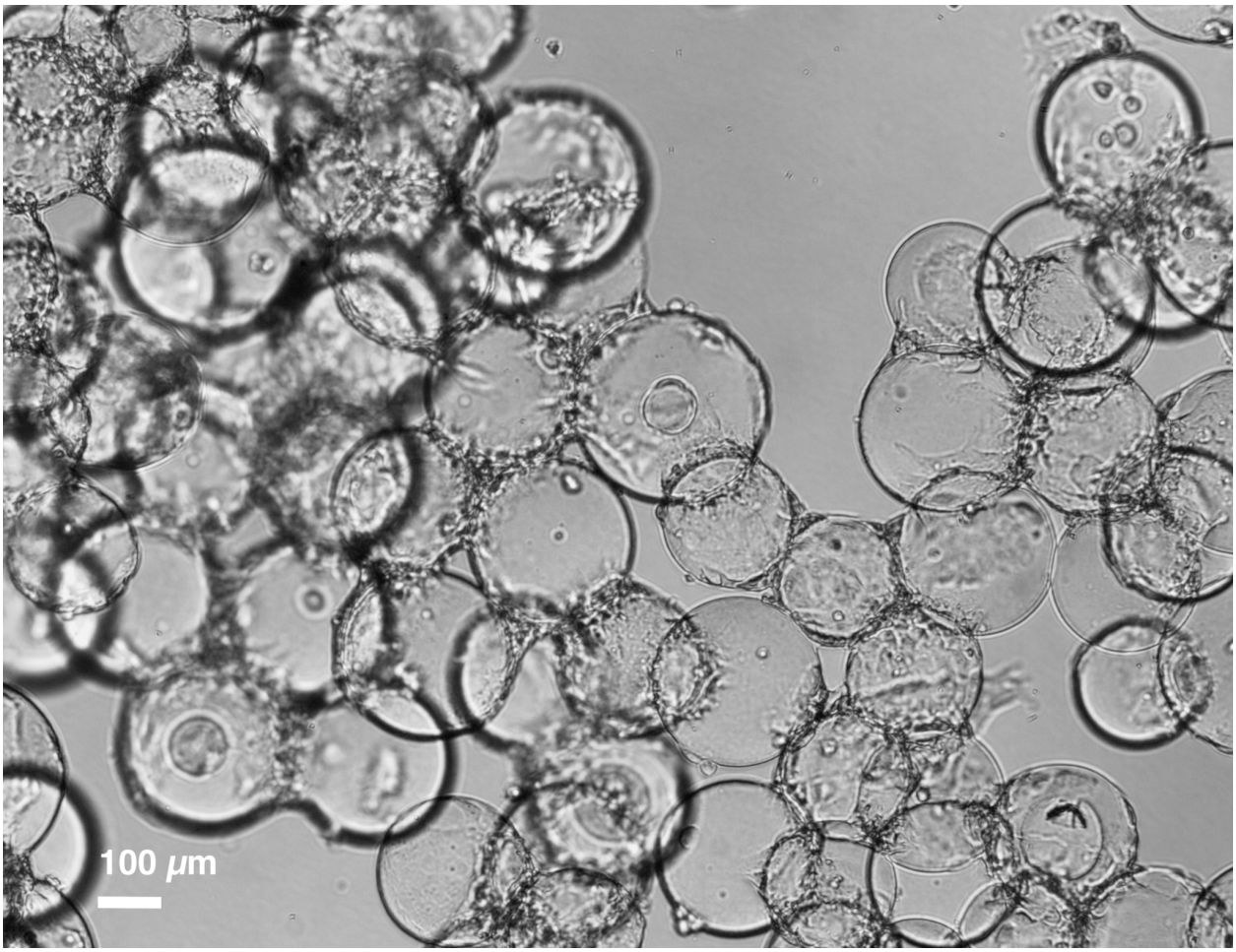
100 μm

Calcein AM, a live cell imaging dye (fluorescing green), were analyzed using fluorescence microscopy (**Fig 6A**). The cells exhibited green fluorescence, indicating that they were viable. Flow cytometry analysis of cell viability on commercial microcarriers, with live cells stained with Calcein AM and dead cells stained with Live-or-Dye, showed that the fluorescence signal of the cell population on microcarriers agreed with the higher green fluorescence signal of live cells and not with the higher red fluorescence signal of dead cells (**Fig 6B-C**). The green fluorescence signal of the live cell control and cells on microcarriers was 100-fold higher than that of the dead cell control (**Fig 6B**). Meanwhile, the red fluorescence signal of the dead cell control was 100-fold higher than that of the live cell control and cells on microcarrier.

Cell viability on microcarriers was established with two different assays that measure distinct cellular characteristics. The Calcein AM stain is an enzymatic live cell dye where intracellular esterases cleave the acetoxymethyl (AM) ester to produce Calcein, a fluorescent dye impermeable to the cell membrane[40]. Dead cells do not retain Calcein due to their compromised cell membranes. The Live-or-Dye viability stain is an amine-reactive dye that does not permeate live cells with intact membranes. However, the dye permeates dead cells with compromised membranes and covalently labels free amines on intracellular proteins[41]. The live cell control and microcarrier culture assay results reflected their difference in viability from the dead cell control. Because the fluorescence signal of the live cell control and cells on microcarriers were overlapping and distinct from that of the dead cell control, we can conclude that cells on microcarriers are viable.

Establishing robust cell signaling from cells grown on microcarriers is essential

Figure 6. Cell viability on commercial microcarriers

A Fluorescence microscopy images of HEK293 cells grown on commercial Cytodex 1 dextran microcarriers and stained with Calcein AM (live cells) yields green fluorescent cells, indicating that cells are viable. **B** Cells are stained with Calcein AM, which will indicate live cells through green fluorescence. Live cells and cells on microcarriers have a 100-fold higher green fluorescence signal than dead cells and blank microcarriers, suggesting that cells on microcarriers are viable. **C** Cells are stained with Live-or-Dye, which indicates dead cells through red fluorescence. Dead cells and blank microcarriers have a 100-fold higher red fluorescence signal than live cells and cells on microcarriers, suggesting that cells on microcarriers are not dead.

A

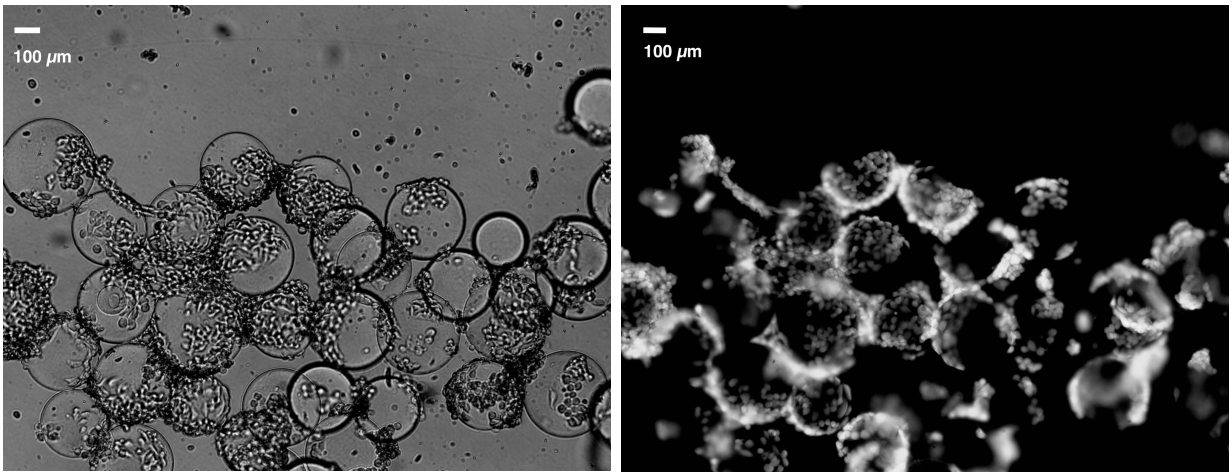
100 μm
100 μm

B

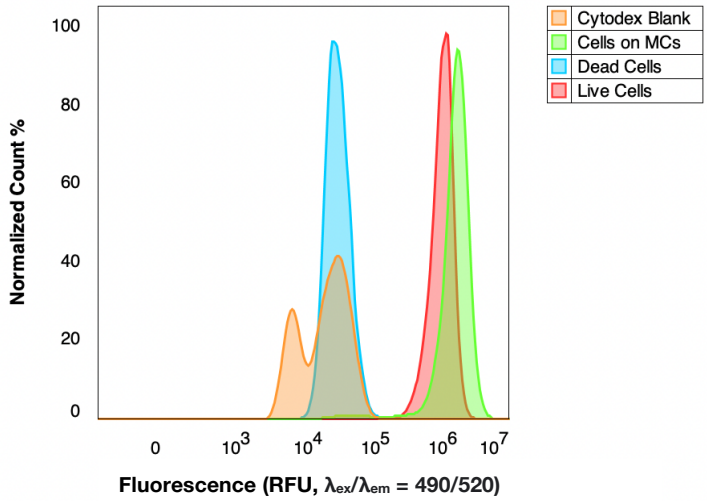
Cytodex Blank
Cells on MCs
Dead Cells
Live Cells
Normalized Count %
100
80
60
40
20
0
0
10^3
10^4
10^5
10^6
10^7
Fluorescence (RFU, λex/λem = 490/520)

C

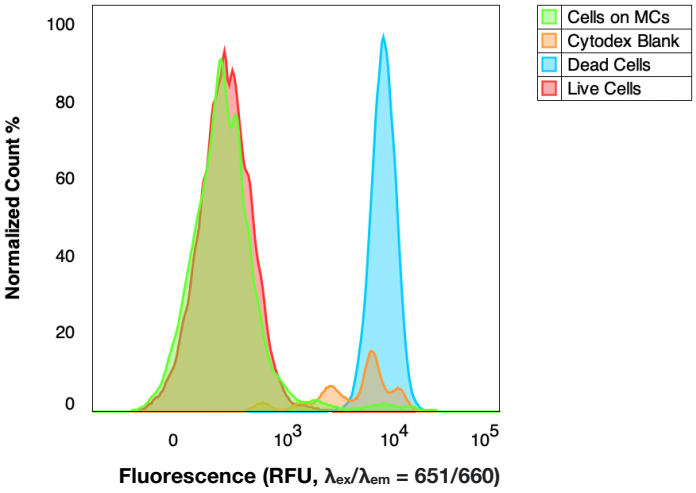
Cells on MCs
Cytodex Blank
Dead Cells
Live Cells
Normalized Count %
100
80
60
40
20
0
0
10^3
10^4
10^5
Fluorescence (RFU, λex/λem = 651/660)

for our proof-of-concept. Cells (10^5) were seeded and grown in a 24-well plate, either on the bottom surface of the well or on microcarriers in the well, and treated with positive control STING agonist DMXAA. Media was then collected and assayed for cell signaling by detecting SEAP activity. Cells grown on microcarriers and treated with DMXAA have detectable cell signaling compared to cells grown and treated in a 24-well plate (**Fig 7**). Although 24 h DMXAA treatment produced barely detectable signal compared to DMSO treatment in cells grown on microcarriers, 48 h DMXAA treatment of cells grown on microcarriers produced signal that was 34% of that seen from cells grown in a well and treated for 24 h.

Culturing cells on microcarriers does not compromise their ability to signal in response to agonist treatment. The cells were seeded at the same density in the bottom of the well plate or on microcarriers, therefore we expected comparable levels of signaling. However, signaling from cells cultured on microcarriers was distinctly lower than signaling from cells cultured in a well plate. This may be due to cells reaching confluency on microcarriers sooner than in the well plate, leading to decreased cell proliferation on microcarriers and a lower final cell count. Cell exposure to compound is also limited in microcarrier culture compared to well plate culture, which may have been a factor in the lower cell signal. Nonetheless, cells cultured on microcarriers still produced detectable SEAP signal, thus we conclude that microcarrier culture is not intrinsically incompatible with a model cell-based assay. This result was a critical proof of concept moving toward our hypothetical microcarrier DEL screening paradigm.

Figure 7. Cell signaling on commercial microcarriers

Cells on microcarriers signal by producing the SEAP reporter gene when stimulated with positive control agonist DMXAA (100 μM). SEAP activity is detected with substrate fluorescein diphosphate (FDP). **A** Cells grown on microcarriers produce detectable signal compared to cells grown on a well plate when treated with DMXAA. **B** Cells grown on microcarriers and treated with DMXAA for 24 h produce a barely detectable signal compared to cells with DMSO treatment. 48 h DMXAA treatment of cells on microcarriers produces a more robust signal, 34% of the signal from cells grown in a well plate. Treatment groups are reproduced in triplicate (n=3). Error bars indicate standard deviation of the mean.

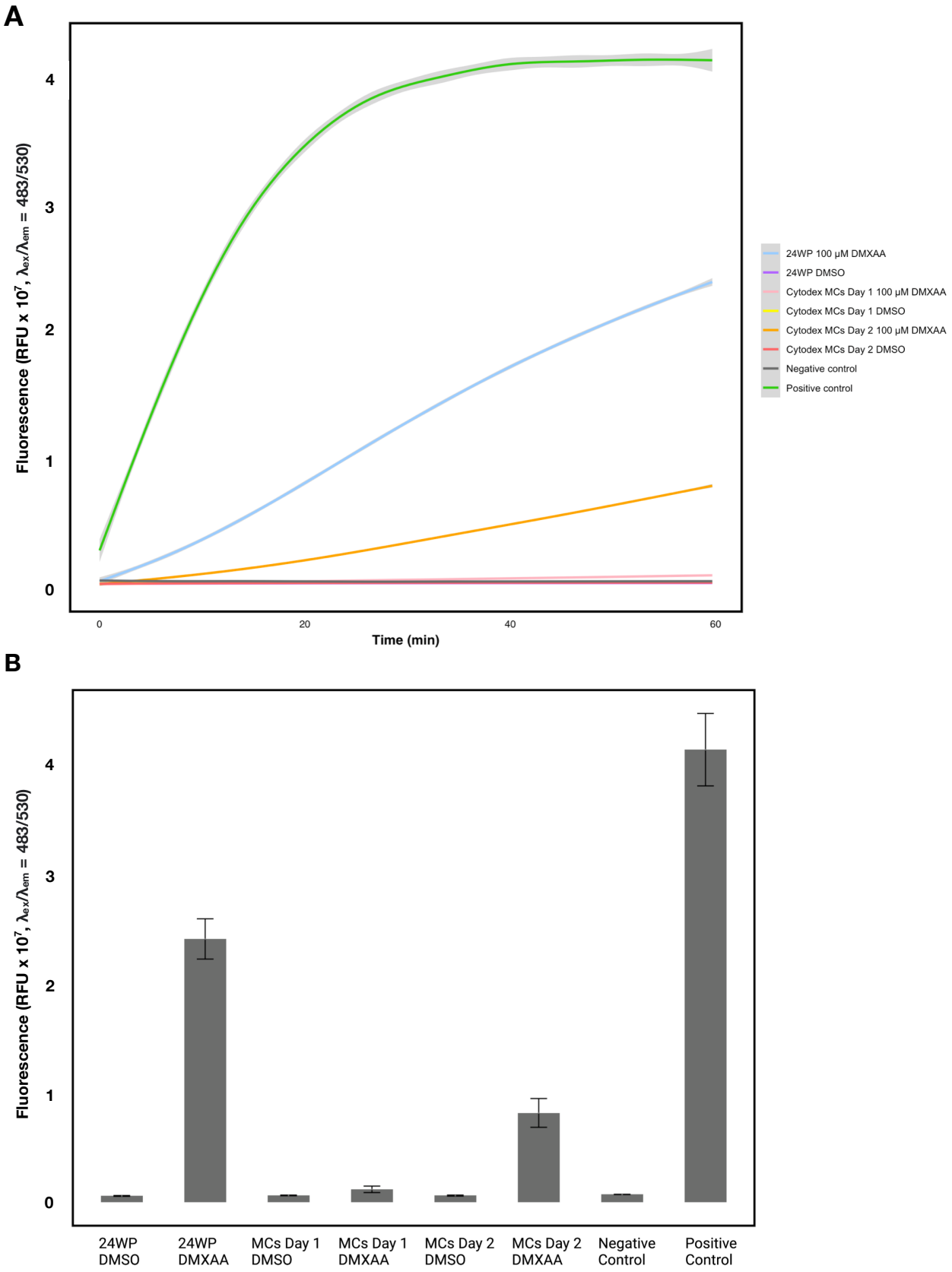
A
Fluorescence (RFU x 10^7, λex/λem = 483/530)
0
1
2
3
4
0
20
40
60
Time (min)
24WP 100 µM DMXAA
24WP DMSO
Cytodex MCs Day 1 100 µM DMXAA
Cytodex MCs Day 1 DMSO
Cytodex MCs Day 2 100 µM DMXAA
Cytodex MCs Day 2 DMSO
Negative control
Positive control
B
Fluorescence (RFU x 10^7, λex/λem = 483/530)
0
1
2
3
4
24WP DMSO
24WP DMXAA
MCs Day 1 DMSO
MCs Day 1 DMXAA
MCs Day 2 DMSO
MCs Day 2 DMXAA
Negative Control
Positive Control

Finding the Optimal Positive Control Agonist

Selecting an appropriate positive control compound is important for any assay development project. In our proposed workflow, cells must signal in response to a photocleaved compound as a model for a cell-based DEL screening paradigm that is analogous to our lab's biochemical activity-based DEL screening strategy[11]. As an added constraint, photocleavage must not be cytotoxic or induce photochemistry in the control compound. Further, photocleaved compound must permeate the cell and initiate signaling before diffusing away into the bulk culture media. These constraints guided agonist selection in investigations of compound photostability and dosing kinetics.

The first positive control agonist we examined was the murine STING agonist, DMXAA. Cells were plated in a 24-well plate, and media was collected 24 h post treatment. Cell signaling after DMXAA pulse dose treatment (100 μM) for various dosing times (20 min, 1 h, 2 h) was compared to 24 h treatment (**Fig 8A**). Treatment for 20 min yielded 25% of signal, and treatment for 1 h yielded 50% signal, compared to treatment for 24 h (**Fig 8B**). DMXAA treatment for 20 min produced a detectable cell signal, but not as robust signaling as 24 h treatment.

The pulsed dosing experiments were designed to test the hypothesis that even transient exposure to DMXAA would result in durable changes to the cells' transcriptional programming, resulting in SEAP signaling. DMXAA treatment induced acceptable cell signal even at lower dosing timepoints. Although DMXAA is a murine STING ligand, our commercial hSTING A162 cell line expresses a modified STING variant that DMXAA agonizes[42]. Because treatment with lower dosing times still

Figure 8. DMXAA-induced cell signaling

hSTING A162 cells were treated with agonist DMXAA (100 μM) for varying times to simulate photodosing conditions. **A** Cells were treated with DMXAA for 20 min, 1 h, 2 h, and 24 h and media was collected and assayed 24 h after initial treatment begins. SEAP activity was assayed with FDP, and reaction progress curves are shown. **B** Endpoints of SEAP activity assays are plotted with error bars indicating the standard deviation of the mean. Treatment groups were reproduced in triplicate (n=3.

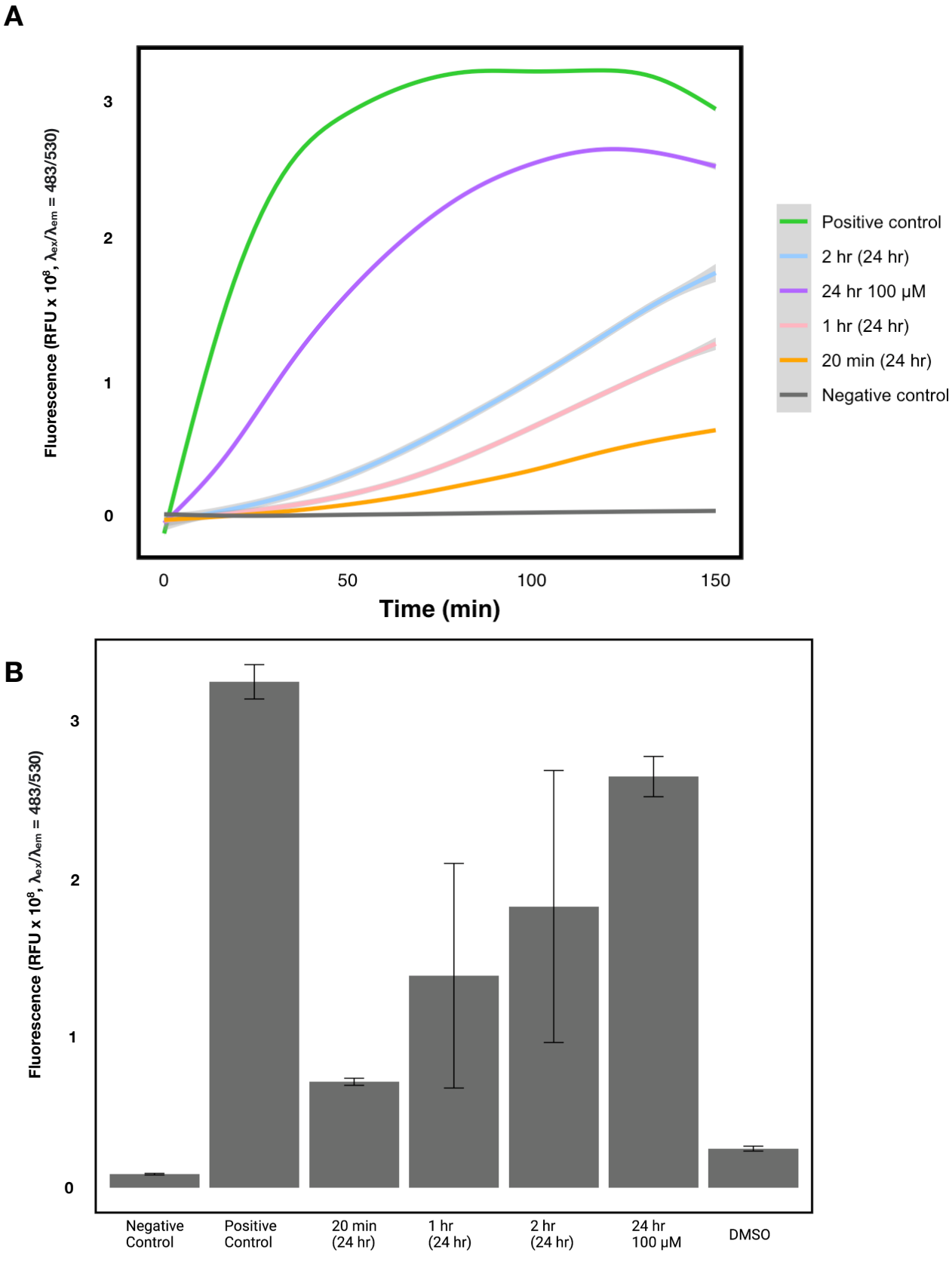
A
Fluorescence (RFU x 10^8, λex/λem = 483/530)
3
2
1
0
0
50
100
150
Time (min)
Positive control
2 hr (24 hr)
24 hr 100 µM
1 hr (24 hr)
20 min (24 hr)
Negative control
B
Fluorescence (RFU x 10^8, λex/λem = 483/530)
3
2
1
0
Negative Control
Positive Control
20 min (24 hr)
1 hr (24 hr)
2 hr (24 hr)
24 hr 100 µM
DMSO

produced detectable signal, DMXAA was plausible positive control ligand for our workflow.

We next sought to study the photochemical stability of DMXAA under conditions of photocleavage. Micrographs suggested that DMXAA crystallized upon UV irradiation (360 nm, 1 h) in both cell culture and in blank media (**Fig 9A**). LCMS analysis of DMXAA standard and DMXAA in media without UV treatment yielded the same extracted ion chromatogram (XIC) profile and UV absorbance (283 m/z, 243 nm), but LCMS analysis of DMXAA in media with subsequent UV irradiation (360 nm) revealed the presence of a new species with m/z = 239, but otherwise identical 243 nm absorbance maximum (**Fig 9B**).

The LCMS analysis of the UV-irradiated DMXAA sample strongly suggested that a photochemical reaction occurred. The most parsimonious explanation of the -44 m/z shift is photochemical decarboxylation. The photoproduct appeared to be insoluble, also in agreement with a decarboxylation, which would yield a much less water-soluble product. Finally, the xanthone chromophore would have remained intact, preserving UV absorbance. Prior structure-activity relationship studies[43] showed that the carboxylic acid is needed to bind and activate STING, therefore these results suggested that DMXAA would likely be unusable as our positive control agonist.

We next turned to SR-717[44] as a possible agonist. Signaling was not observed using the hSTING A162 cell line, so another STING isoform with the wild-type hSTING R232 was used[45]. Cell signaling after SR-717 pulse dose treatments (100 μM) for several different times (20 min, 1 h, 2 h, 24 h) was compared (**Fig 10A**), normalizing to

Figure 9. DMXAA photochemistry

A DMXAA (100 μM) was added to HEK293 cell culture and blank media in 24-well plates and treated with UV irradiation (365 nm) for 1 h. After UV irradiation of DMXAA in both cell culture and blank media, black crystals were observed in brightfield microscopy micrographs. **B** LC-MS analysis was conducted on the DMXAA stock and on DMXAA solutions in media with and without UV irradiation. Extracted ion chromatograms (XIC) and absorbance detection (243 nm) were used to monitor eluent.

A

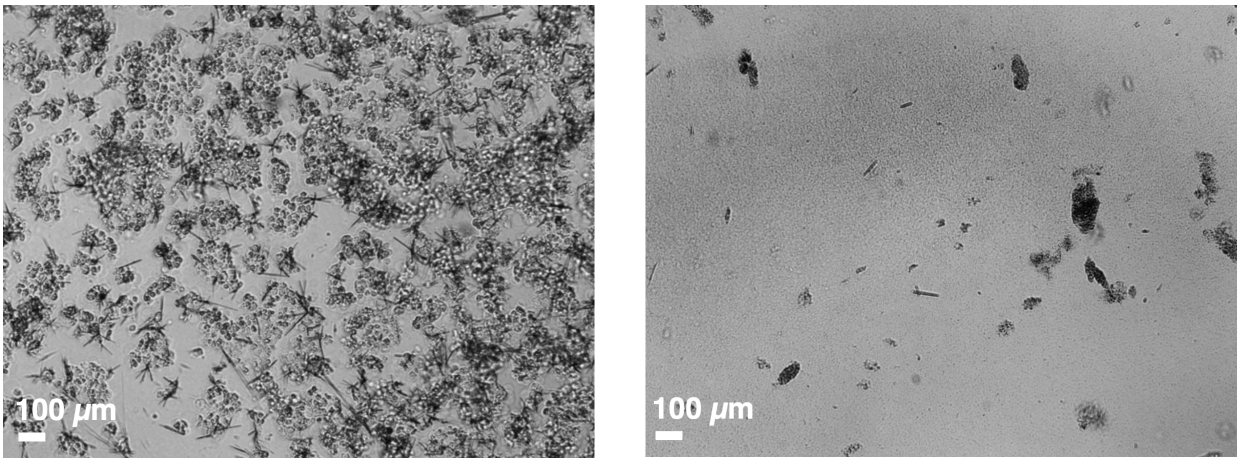
100 μm
100 μm

B

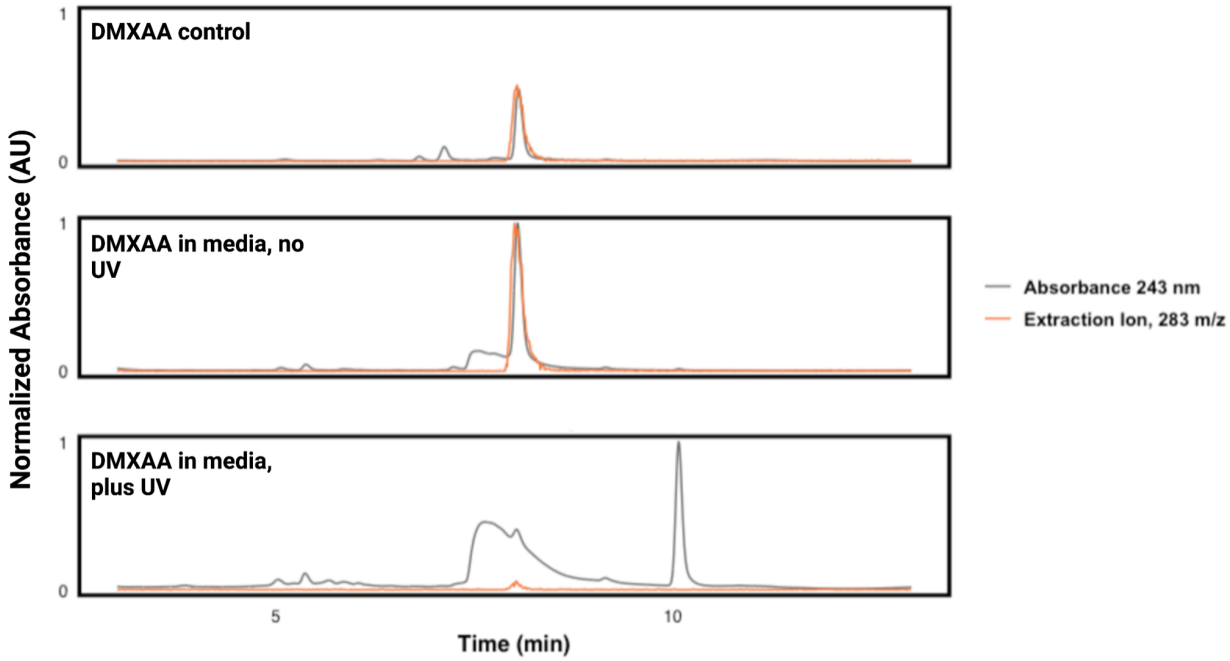
DMXAA control
DMXAA in media, no UV
DMXAA in media, plus UV
Normalized Absorbance (AU)
1
0
5
10
Time (min)
Absorbance 243 nm
Extraction Ion, 283 m/z

Figure 10. SR-717-induced cell signaling

hSTING R232 cells were treated with SR-717 (100 μM) for varying times to simulate photodosing conditions. **A** Cells were treated with SR-717 for 1 h, 2 h, and 24 h and media was collected and assayed 24 h after initial treatment begins. SEAP activity was assayed with FDP, and reaction progress curves are shown. **B** Endpoints of SEAP activity assays are plotted with error bars indicating the standard deviation of the mean. Treatment groups are reproduced in triplicate (n=3).

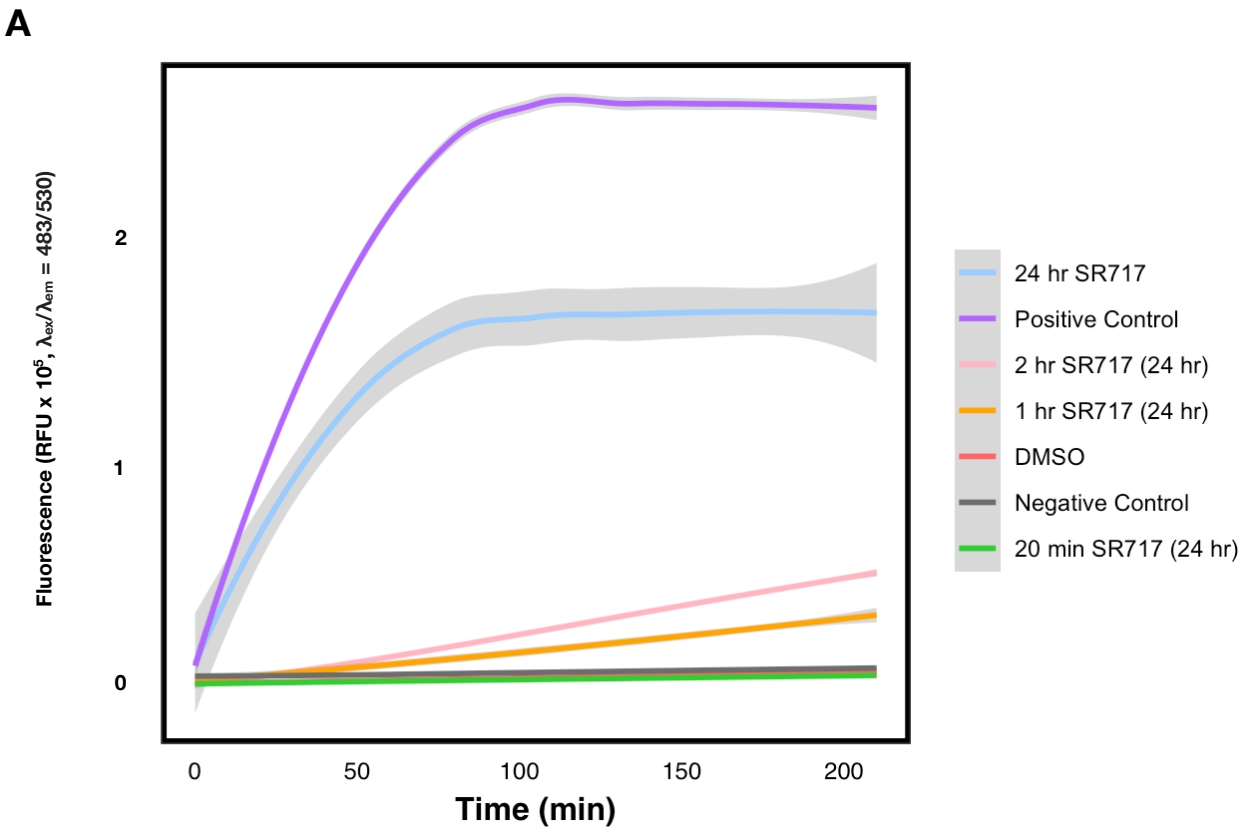
A
Fluorescence (RFU x 10^5, λex/λem = 483/530)
2
1
0
0
50
100
150
200
Time (min)
24 hr SR717
Positive Control
2 hr SR717 (24 hr)
1 hr SR717 (24 hr)
DMSO
Negative Control
20 min SR717 (24 hr)

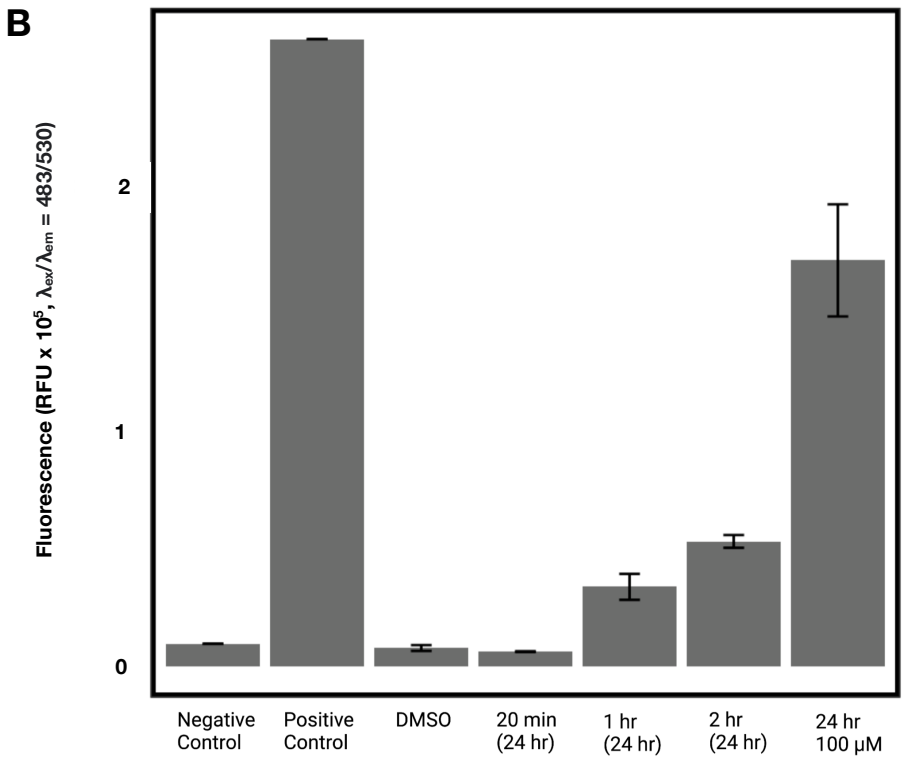
B
Fluorescence (RFU x 10^5, λex/λem = 483/530)
2
1
0
Negative Control
Positive Control
DMSO
20 min (24 hr)
1 hr (24 hr)
2 hr (24 hr)
24 hr 100 µM

signaling observed after 24 h SR-717 treatment. SR-717 treatment for 1 h produced 20% cell signal, treatment for 2 h produced 31% cell signal, and treatment for 20 min produced no detectable signal (**Fig 10B**).

SR-717 was an attractive option for our positive control agonist. It would be easily synthesized as a DEL-like compound using commercially available Fmoc-protected amino acid and carboxylic acid building blocks. Importantly, SR-717 is a human (not murine) STING agonist, allowing the use of the human STING target for screening. Also, given its structure, it would be unlikely to undergo spurious photochemistry. However, SR-717 was not a robust agonist. Higher concentrations of SR-717 and longer treatment times (1 h) were required to detect STING signaling. With no detectable signal at 20 min treatment, this agonist would have made microcarrier dosing experiments more difficult. Thus, SR-717 was not an ideal candidate for our tool compound although it will make an excellent positive control in a first DEL and generally serves as good inspiration for DEL design.

We finally examined MSA-2[46] as a potential positive control agonist. MSA-2 treatment at 10 and 30 μM for 24 h produced comparable, high levels of SEAP signal (**Fig 11A**) compared to 100 μM MSA-2 treatment for 24 h. Treatment with 10 μM MSA-2 produced 100% cell signal, and 30 μM MSA-2 treatment produced 108% cell signal (**Fig 11B**).

We also explored pulsed MSA-2 dosing to simulate DEL photocleavage-based dosing as described previously. MSA-2 treatment (100 μM, 20 min) produced comparable cell signal to treatment for 24 h (**Fig 12A**). Treatment for 1 and 2 h produced a higher signal than treatment for 24 h. Cell signaling from MSA-2 treatment

Figure 11. MSA-2-induced cell signaling at varying concentrations

hSTING R232 cells were treated with MSA-2 for 24 h at varying concentrations to determine efficacy of compound in signaling induction. **A** Cells were treated with 10, 30, and 100 μM MSA-2 for 24 h and media is collected and assayed 24 h after initial treatment begins. SEAP activity was assayed with FDP, and reaction progress curves are shown. **B** Endpoints of SEAP activity assays are plotted with error bars indicating the standard deviation of the mean. Treatment groups are reproduced in triplicate (n=3).

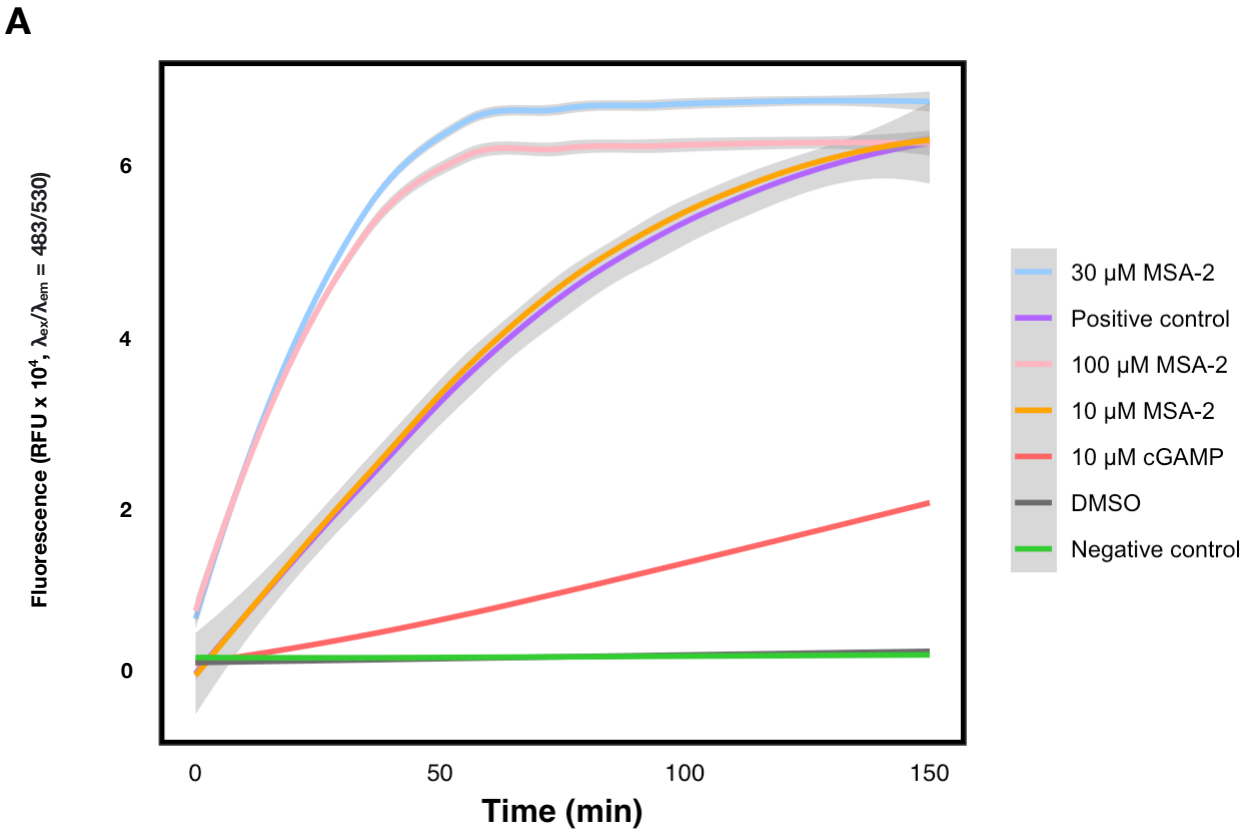
A
Fluorescence (RFU x 10⁴, λex/λem = 483/530)
6
4
2
0
0
50
100
150
Time (min)
30 μM MSA-2
Positive control
100 μM MSA-2
10 μM MSA-2
10 μM cGAMP
DMSO
Negative control

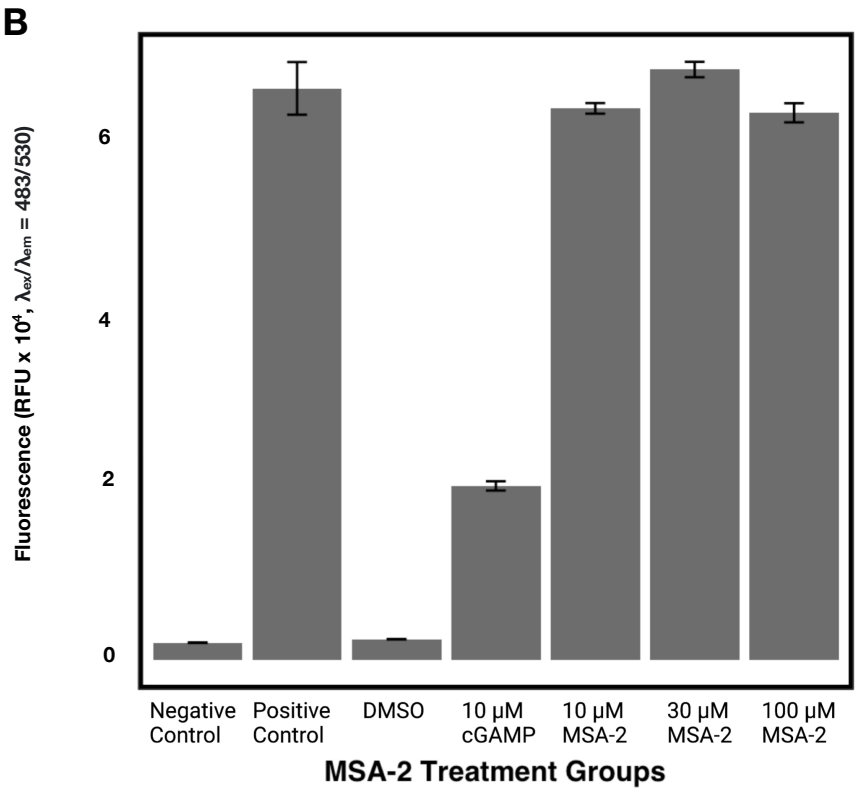
B
Fluorescence (RFU x 10⁴, λex/λem = 483/530)
6
4
2
0
Negative Control
Positive Control
DMSO
10 μM cGAMP
10 μM MSA-2
30 μM MSA-2
100 μM MSA-2
MSA-2 Treatment Groups

Figure 12. MSA-2-induced cell signaling at varying treatment times

hSTING R232 cells were treated with MSA-2 (100 μM) for varying times to simulate photodosing conditions. Transient stimulation (20 min) with MSA-2 induces robust STING signaling. **A** Cells were treated with 100 μM MSA-2 for 20 min, 1 h, 2 h, and 24 h and media was collected and assayed 24 h after initial treatment begins. SEAP activity was assayed with FDP, and reaction progress curves are shown. **B** Endpoints of SEAP activity assays are plotted with error bars indicating the standard deviation of the mean. Treatment groups are reproduced in triplicate (n=3).

A

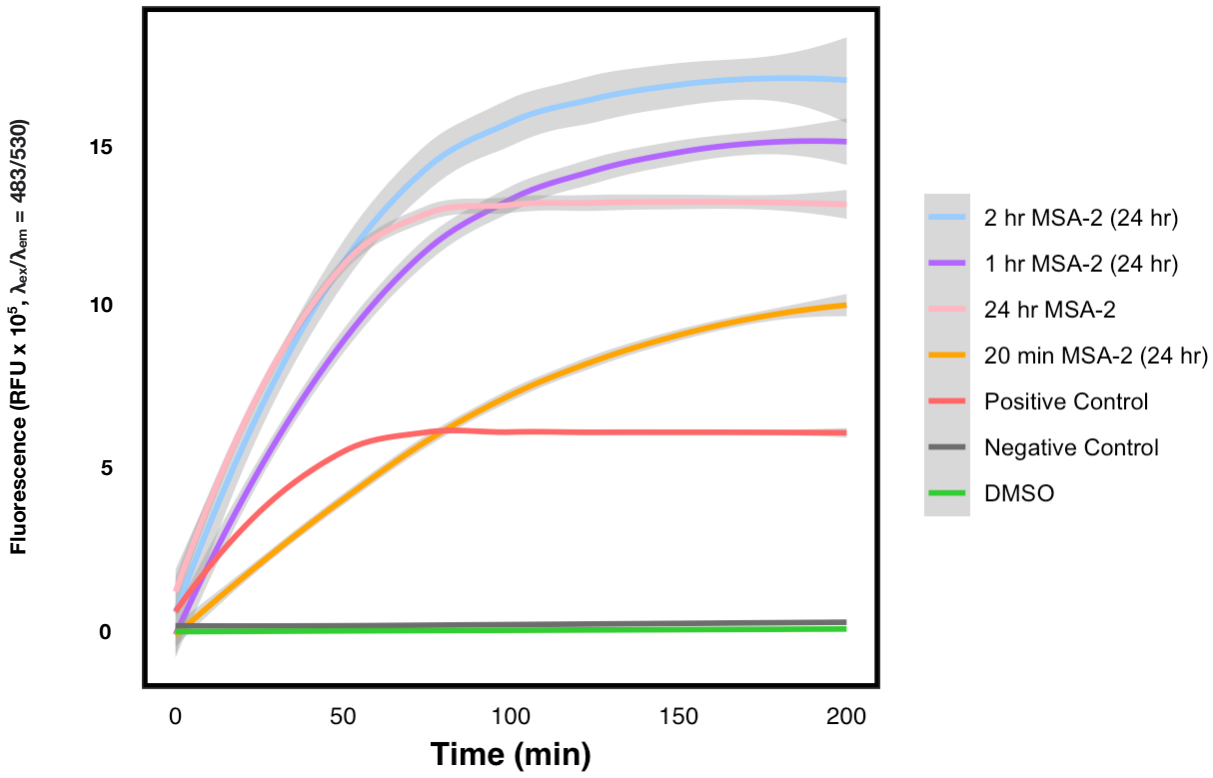
Fluorescence (RFU x 10^5, λex/λem = 483/530)
15
10
5
0
0
50
100
150
200
Time (min)
2 hr MSA-2 (24 hr)
1 hr MSA-2 (24 hr)
24 hr MSA-2
20 min MSA-2 (24 hr)
Positive Control
Negative Control
DMSO

B

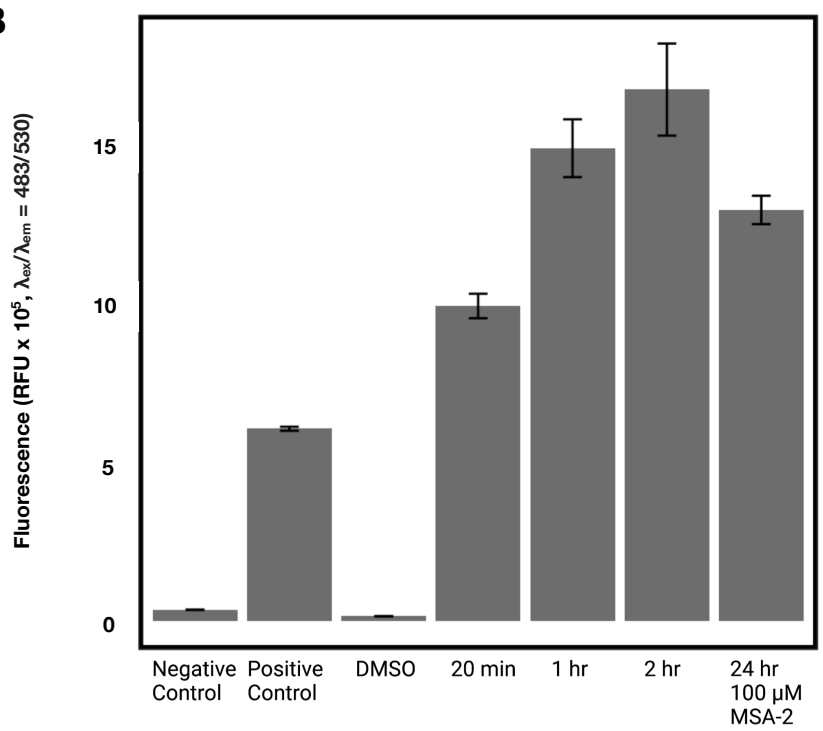
Fluorescence (RFU x 10^5, λex/λem = 483/530)
15
10
5
0
Negative Control
Positive Control
DMSO
20 min
1 hr
2 hr
24 hr 100 µM MSA-2

for 20 min was 77% of the signal seen with 24 h dosing, and cell signal from treatment for 1 and 2 h was 115 and 129% of the signal from treatment for 24 h, respectively (**Fig 12B**).

MSA-2 potently agonized STING in both dose-escalation and pulsed dosing experiments. MSA-2 treatment produced strong signal even at shorter treatment times and at lower concentration, ideal pharmacological properties for our proposed workflow. Like DMXAA and SR-717, MSA-2 also contains a carboxylic acid, making it very straightforward to prepare photocleavable MSA-2 beads. MSA-2 was ultimately found to be the best tool compound to progress into photodosing studies on microcarriers. Moving forward, we must test MSA-2 for photostability. It is possible that its structure will also absorb UV, though the ethyl linker makes decarboxylation unlikely.

Assessing Cell Viability from Photocleavage Conditions

Cell viability in compound photocleavage conditions is an important consideration for our workflow. We intend to grow cells on microcarriers that also display photocleavable tool compound, which will be liberated using UV light to stimulate the cells on the microcarrier. UV exposure can be cytotoxic depending on wavelength and exposure time[47]. Thus, we set out to explore these parameters in the context of cell viability assays.

We first investigated whether irradiation using our UV source, Analytik Jena's UVP crosslinker oven (365 nm), would elicit a cytotoxic response. Cells were irradiated for 20 min and 1 h. Live cells were stained with Calcein AM, dead cells were stained with Live-or-Dye, and populations were quantified via flow cytometry. Treatment for 1 h in the oven completely compromised cell viability, while treatment for 20 min reduced viability 50% compared to the live cell control (**Fig 13**).

We further investigated whether the cytotoxic response was related to irradiation or heating. Encasing the cells in foil before UV exposure preserved 100% viability compared to that of control live cells (**Fig 14A**). Placing the cells on ice during UV exposure nearly completely compromised viability compared to that of control live cells (**Fig 14B**). Quantitatively, cells protected with foil during UV irradiation were as viable as control live cells, and cells placed on ice during irradiation were almost completely nonviable compared to control live cells.

UV irradiation using our crosslinking oven adversely affected cell viability. Covering the cells in foil during UV exposure protects against cytotoxicity entirely, although the results are confounded for our investigation of whether cytotoxicity was

Figure 13. Cell viability assays of 365-nm UV irradiation

Cell viability was assayed with Live-or-Dye fixable viability stain after 1-h treatment in 365 nm UV oven. **A** The UV source was a UV oven from Analytik Jena: UVP Crosslinker CL - 1000L 365 nm. **B** Cells cultured in a 6-well plate were treated with UV irradiation for 20 min and 1 h or left outside the incubator at room temperature for 1 h. Cells were stained with Live-or-Dye 24 h after treatment and analyzed by flow cytometry. Percentage of viable cells compared to the live cell control are plotted with error bars indicating the standard deviation of the mean. Treatment groups are reproduced in duplicate (n=2).

A


UVP Crosslinker
analytikjena

B

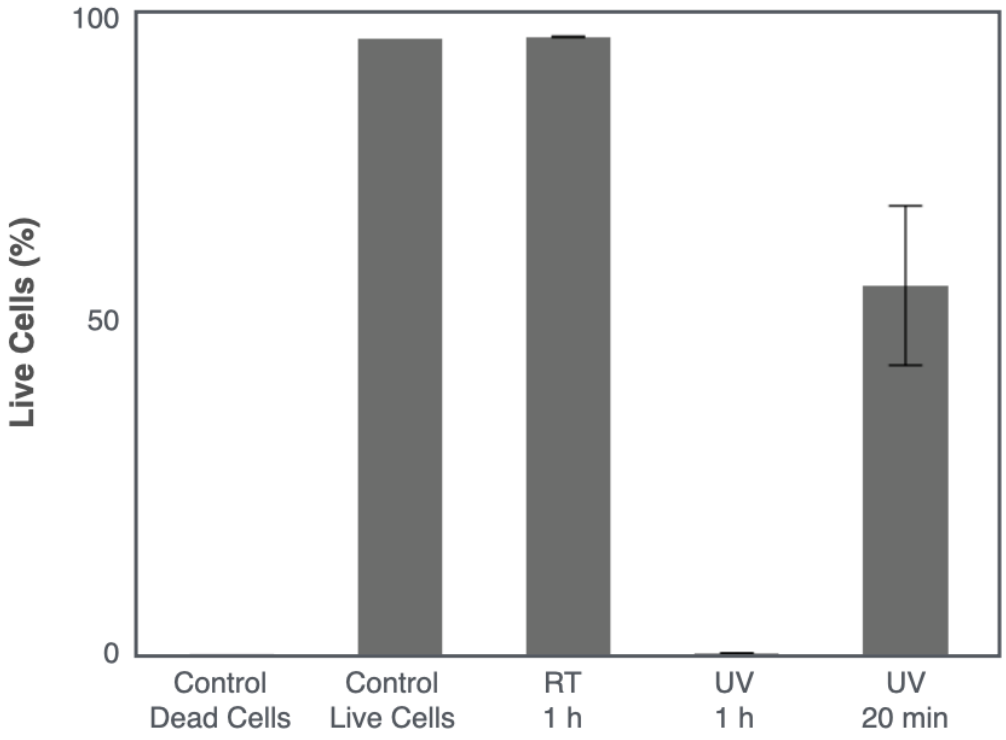
Live Cells (%)
100
50
0
Control
Dead Cells
Control
Live Cells
RT
1 h
UV
1 h
UV
20 min

Figure 14. Cell viability of various UV oven photocleavage conditions

Cell viability was assayed with Live-or-Dye fixable viability stain after 1-h treatment in 365 nm UV oven with foil coverage or ice treatment to assess whether heat from UV oven or UV exposure led to cytotoxicity. **A** Cells cultured in a 6-well plate were wrapped in foil and treated with UV irradiation for 1 h. Cells were stained with Live-or-Dye 24 h after treatment and analyzed by flow cytometry. Percentage of viable cells compared to the live cell control are plotted with error bars indicating the standard deviation of the mean. Treatment groups are reproduced in duplicate (n=2). **B** Cells cultured in a 6-well plate were placed on ice and treated with UV irradiation for 1 h. Cells were stained with Live-or-Dye 24 h after treatment and analyzed by flow cytometry. Percentage of viable cells compared to the live cell control are plotted with error bars indicating the standard deviation of the mean. Treatment groups are reproduced in duplicate (n=2).

A

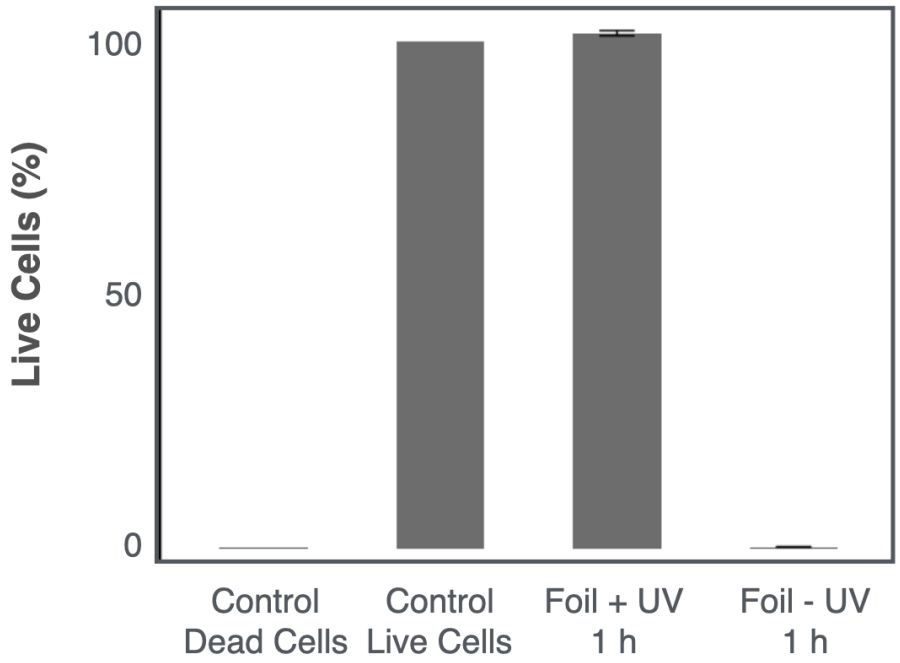
100
50
0
Live Cells (%)
Control
Dead Cells
Control
Live Cells
Foil + UV
1 h
Foil - UV
1 h

B

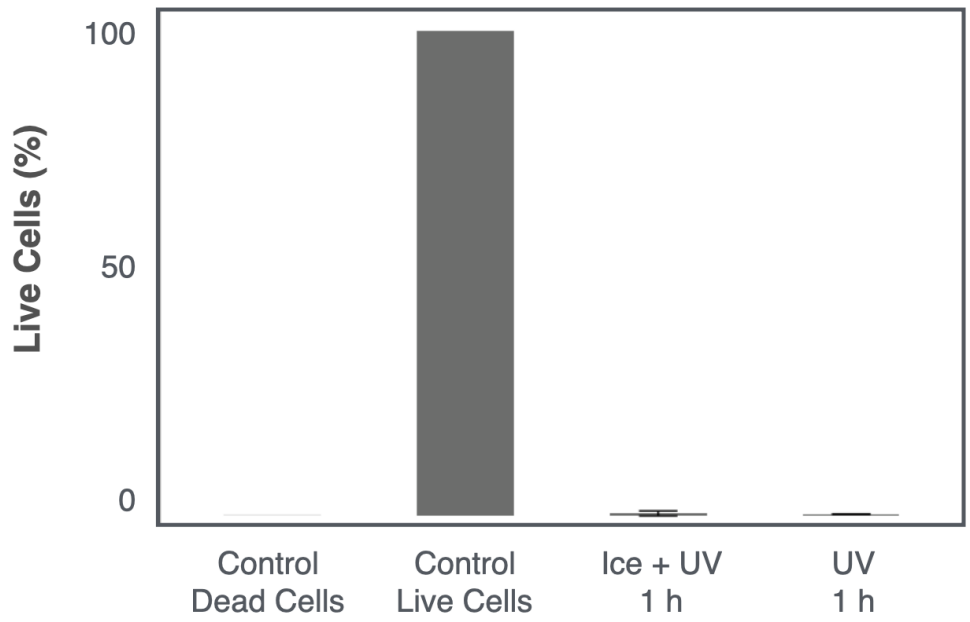
100
50
0
Live Cells (%)
Control
Dead Cells
Control
Live Cells
Ice + UV
1 h
UV
1 h

due to irradiation or heating because foil both blocks UV and acts as a heat sink. However, placing the cells on ice to moderate the temperature during irradiation was not protective against cytotoxicity. Thus, we concluded that UV irradiation was responsible for cytotoxicity, not heating.

We next investigated higher wavelength sources of irradiation, suspecting this might preserve cell viability. Commercial UV LED light strips (385-400 nm) were placed in the incubator (**Fig 15A**). Cell viability after LED irradiation for 1 h was 95% of control live cell viability, whereas viability after 365 nm irradiation was 20% of control live cell viability (**Fig 15b**). LED irradiation did not significantly affect viability compared to that of live cell controls.

To validate the UV-LED photocleavage condition, we generated photocleavable MSA-2 microcarriers and tested whether HEK293 hSTING R232 dual reporter cells signaled in response to photocleaved MSA-2. Cells were grown on the PC-MSA-2 microcarriers and exposed to UV LED treatment for 1 hour, and media was collected and assayed 24 h later for SEAP activity. There was robust cell signal from the UV-treated photocleavable compound group, comparable to the signal from the positive control, and no cell signal was observed in the non-UV-treated group (**Fig 16A**). Signal from the PC-MSA-2 group with UV exposure was 75% of the signal from the positive control (**Fig 16B**).

These experiments demonstrated the feasibility of using a photocleaved STING agonist to induce signaling in cells growing on agonist-displaying microcarriers. Importantly, the compound remained stable on the photolinker and did not induce cell signaling without photocleavage. Furthermore, expanding on earlier findings, cells grew

Figure 15. Cell viability assays of UV-LED exposure

Cell viability assayed with Live-or-Dye fixable viability stain after 1 h treatment with 390 nm UV LED strips. **A** The UV source was UV-LED strips from Ciyoyo, model LED02, 36W 385-400 nm. **B** Cells cultured in a 6-well plate were wrapped in UV-LED strips and treated with UV irradiation for 1 h. Cells were stained with Live-or-Dye 24 h after treatment and analyzed by flow cytometry. Percentage of viable cells compared to the live cell control are plotted with error bars indicating the standard deviation of the mean. Treatment groups are reproduced in duplicate (n=2).

A

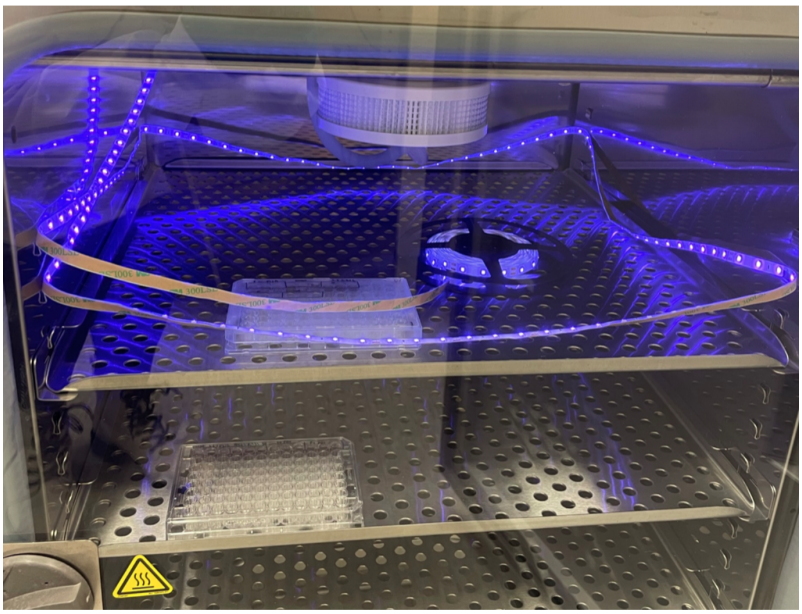

B

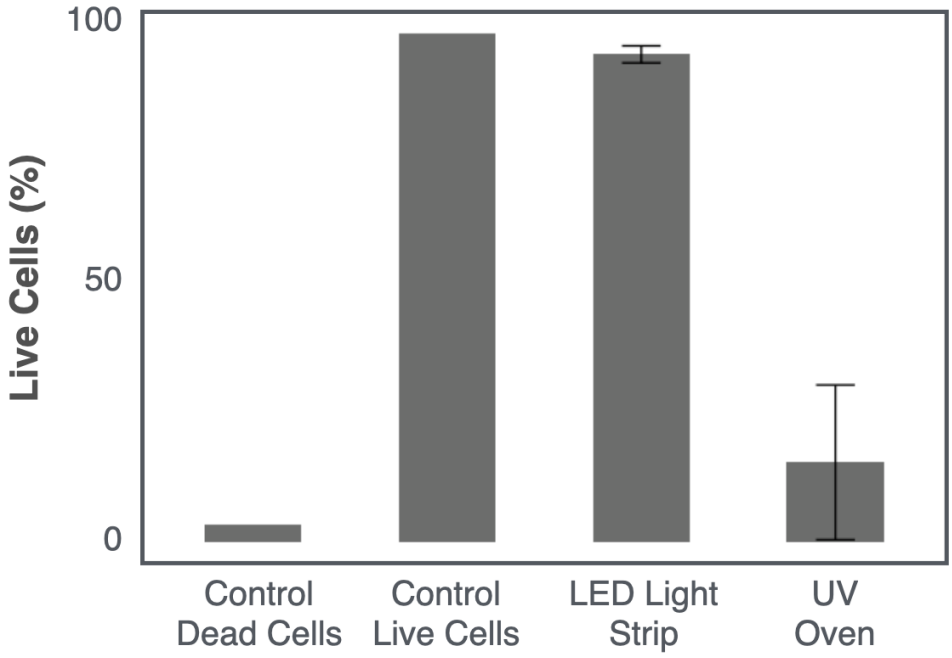
100
50
0
Live Cells (%)
Control
Dead Cells
Control
Live Cells
LED Light
Strip
UV
Oven

Figure 16. Cell signaling from photodosed PC-MSA-2 beads

UV LED irradiation of PC-MSA-2 tool beads induces signaling in HEK293 hSTING R232 reporter cells. **A** Cells grown on PC-MSA-2 beads were treated with UV-LED irradiation for 1 h. Media was collected and assayed 24 h after initial treatment begins. SEAP activity was assayed with FDP, and reaction progress curves are shown. **B** Endpoints of SEAP activity assays are plotted with error bars indicating the standard deviation of the mean. Treatment groups are reproduced in triplicate (n=3).

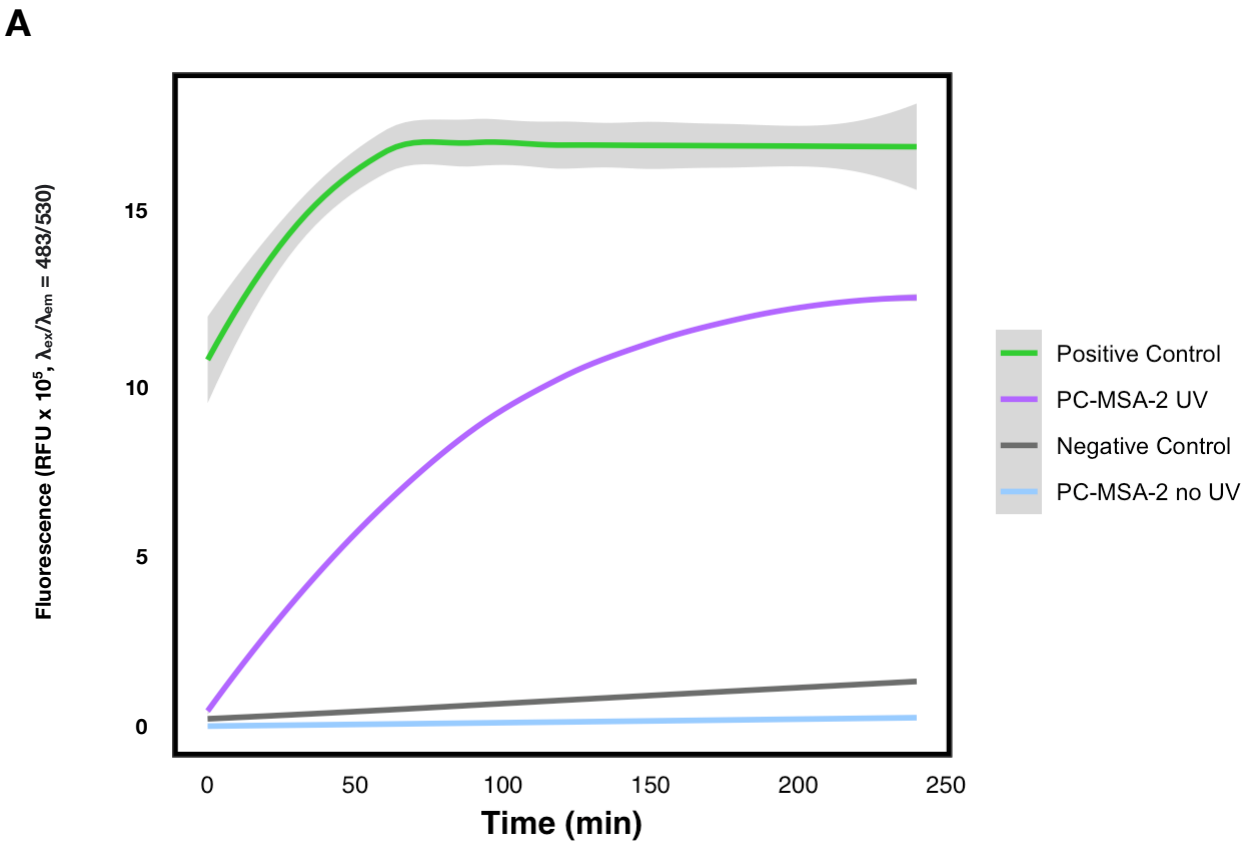
A
Fluorescence (RFU x 10^5, λex/λem = 483/530)
15
10
5
0
0
50
100
150
200
250
Time (min)
Positive Control
PC-MSA-2 UV
Negative Control
PC-MSA-2 no UV

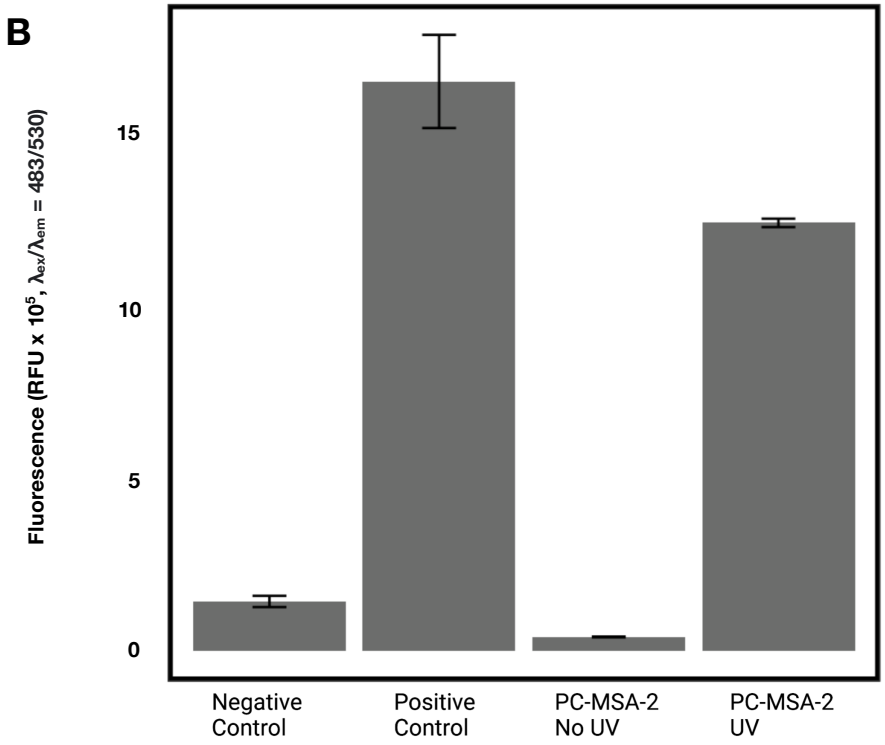
B
Fluorescence (RFU x 10^5, λex/λem = 483/530)
15
10
5
0
Negative Control
Positive Control
PC-MSA-2 No UV
PC-MSA-2 UV

and signaled properly when grown on chemically functionalized microcarrier beads. These studies do not yet confirm that MSA-2 liberated from a microcarrier bead only induced signaling in cells attached to the same microcarrier. Those critical experiments require an IRF3-inducible reporter line compatible with our reporter capture strategy.

Viability studies of photocleavage conditions highlighted the numerous obstacles to adapting the solid-phase DEL screening to cells. We were able to preserve HEK293 cell viability and maintain compound photorelease efficacy using a different UV source. More sensitive cell lines may require greater care. We set up the UV LEDs in an incubator, allowing controlled temperature and CO_2 levels. Additional experiments are now necessary to determine the generality of this approach for other adherent cell lines and whether non-adherent cell types can be used.

Engineering Secreted Protein Reporter Lines with CRISPR/Cas9

With the proof-of-concept assays complete, we turned to evaluating reporter detection in our platform. Our original workflow involved immobilizing SEAP substrates in the hydrogel microcarriers. We considered engineering an affinity-tagged SEAP reporter cell line, but the difficulties of capturing the FDP substrate prompted exploration of alternative approaches. We adapted the proposed workflow by shifting from an enzymatic reporter to a secreted fluorescent protein reporter. In the revised workflow, a cell line would be engineered to secrete a HaloTag-labeled GFP (GFP-Halo[48]) and this line would be cultured on photocleavable tool bead microcarriers displaying the cognate ligand of HaloTag (**Fig 17**). UV irradiation would liberate the tool compound and induce cell signaling in the form of GFP-Halo secretion, and the secreted reporters would be covalently captured, labeling the microcarrier as a positive "hit" that is sortable by FACS.

We first engineered the required constitutive secreted GFP-Halo reporter cells. The constitutive expression cassette structure for stable cell line generation included several key elements (**Fig 18**). The chromatin insulator prevents transcriptional silencing of the vector, and the CAG promoter induces strong, constitutive expression[49]. The WPRE element increases vector expression, and the P2A peptide is a cleavage site that liberates the antibiotic resistance marker from the secreted protein. The cassette is designed to be inserted via CRISPR/Cas9 genome editing[50] into the AAVS1 "safe harbor" locus, a region in the human genome where edits do not affect normal gene expression[51].

Figure 17. GFP-Halo reporter workflow

Proposed cellular DEL screening workflow. Engineered GFP-Halo secreting reporter cells will be grown on tool bead microcarriers encasing the photocleavable compound. Photodosing will result in liberation of the bead compound and induction of cell signaling in the form of reporter secretion. Microcarriers will be functionalized with HaloTag ligand for covalent capture of secreted GFP-Halo protein. Positive “hit” microcarriers will fluoresce green, becoming sortable by FACS.

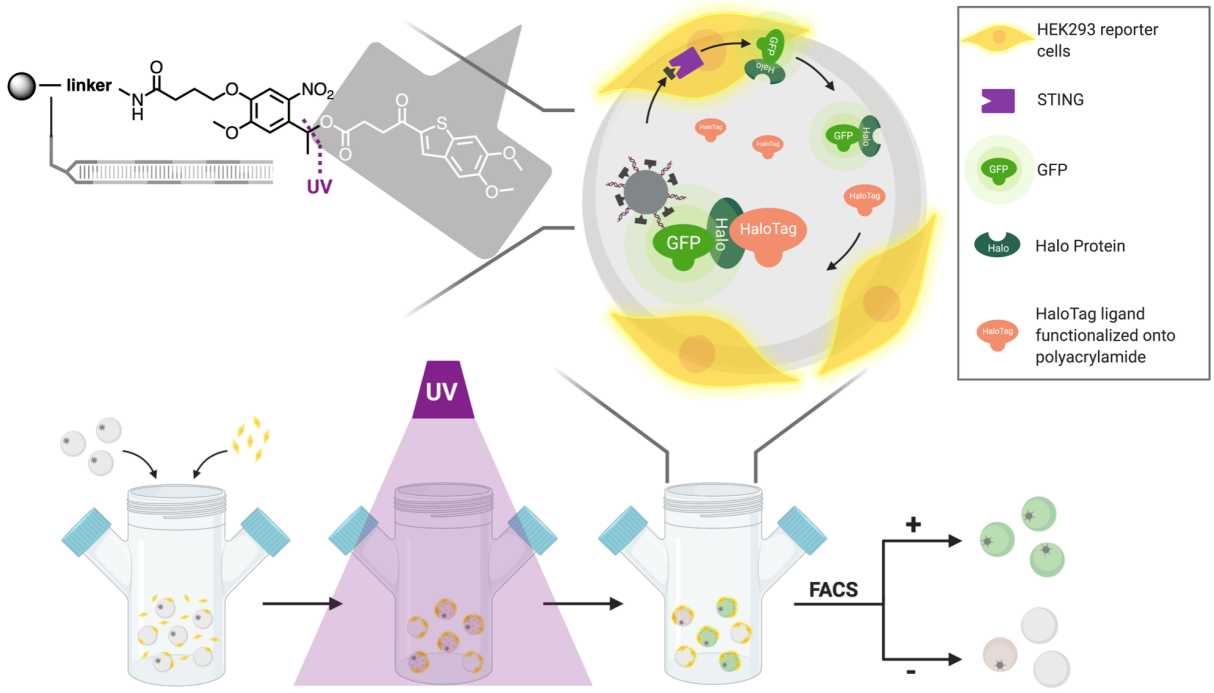

Created with BioRender.com

Figure 18. Stable cell line reporter expression cassette

Constitutive expression cassette structure for stable cell line generation. Elements include chromatin insulator, CAG promoter, WPRE element, and P2A peptide. The cassette is inserted into the AAVS1 “safe harbor” locus.

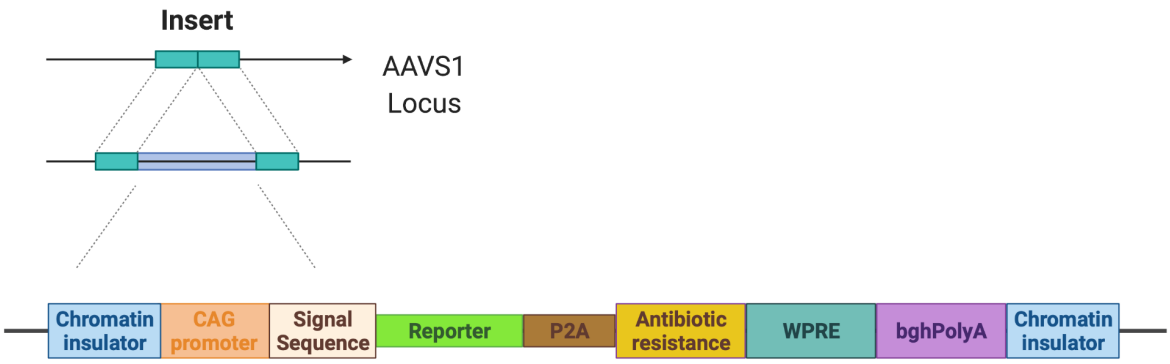

Reporter: GFP-Halo or sfCherry-Halo

We generated a GFP-Halo secreted reporter cell line using HEK293T and HeLa cells. In confocal fluorescence microscopy imaging analysis of the stably transfected HEK293T cells constitutively expressing secreted GFP-Halo, nearly all the cells were fluorescent (**Fig 19A**). Media fluorescence of the secreted GFP-Halo HEK293T cell lines after two days of culture was 22 times higher than the background media fluorescence of wild-type HEK293T cells (**Fig 19B**). When the fluorescence signal of the engineered secreted GFP-Halo cell lines was quantified by flow cytometry, both the HEK293T and HeLa cell lines have a 100-fold higher fluorescence signal than wild-type HEK293T cells (**Fig 19C**).

Microscopy, flow cytometry, and media fluorimetry data collectively supported the conclusion that HEK293T and HeLa cells were successfully transformed with the secreted GFP-Halo. The high fluorescence of engineered cells in confocal microscopy images indicated strong GFP protein expression. Flow cytometry data corroborated that conclusion. Finally, the much higher fluorescence of media from engineered cells compared to that of media from wild-type cells indicated that GFP was efficiently secreted from the cell into the media surroundings. The analyses did not include an assay of HaloTag function, but the data collectively indicated successful generation of the desired new reporter lines.

We also generated a second color reporter comprising an sfCherry-Halo cell line in HEK293T cells using CRISPR/Cas9. The engineered HEK293T cells were highly fluorescent in confocal fluorescence microscopy imaging analysis (**Fig 20A**). Media fluorescence after two days of culture was 25 times higher than the background media fluorescence of wild-type HEK293T cells (**Fig 20C**). The secreted Cherry-Halo

Figure 19. Constitutive GFP reporter

A Constitutive GFP reporter line was imaged with the Leica Stellaris 8 confocal microscope. **B** Media fluorescence was measured after 2 day culture for both transfected and wild-type cells. **C** Transfected and wild-type cells were analyzed by flow cytometry.

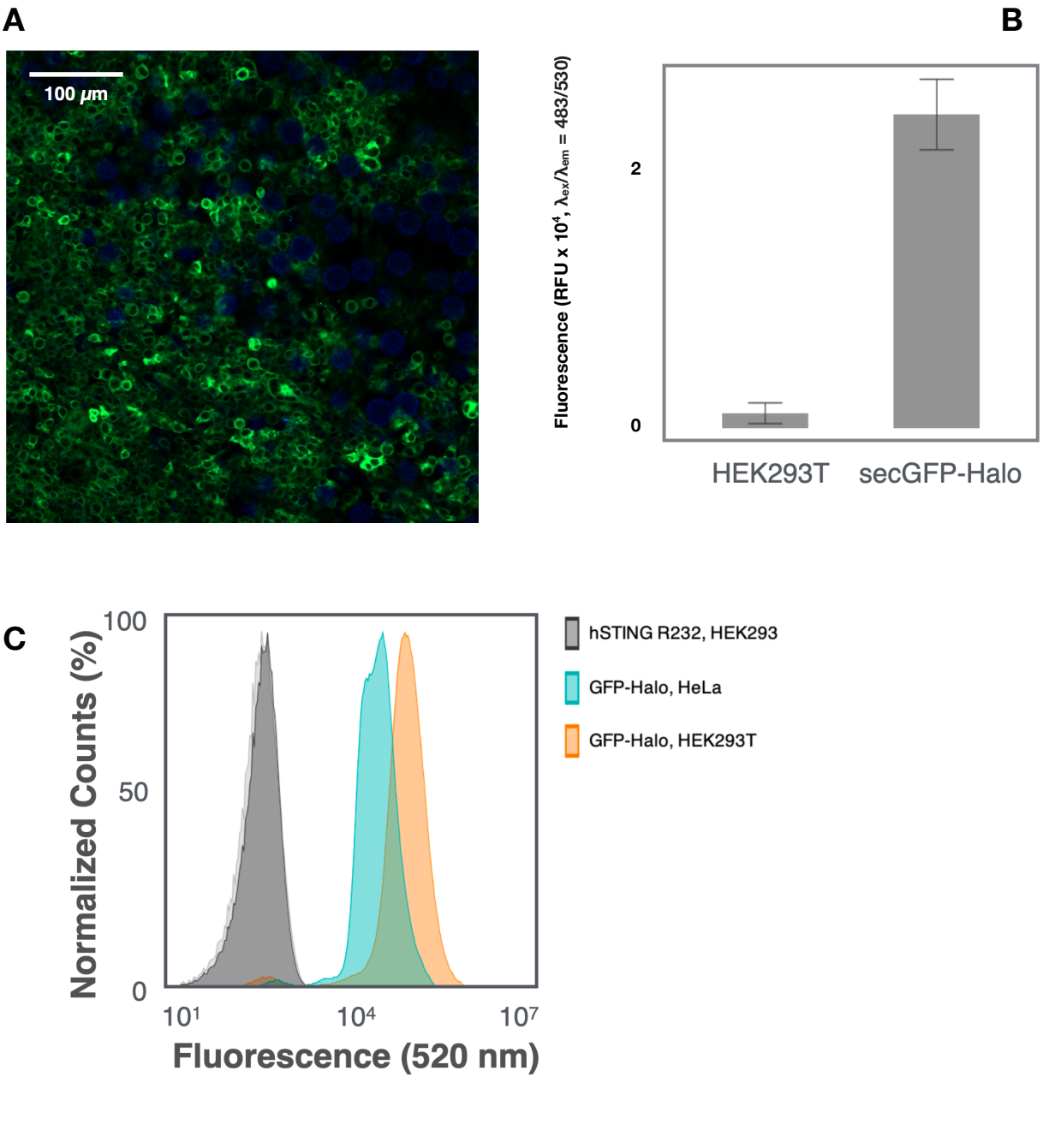
A
100 μm
B
Fluorescence (RFU x 10⁴, λex/λem = 483/530)
2
0
HEK293T
secGFP-Halo
C
Normalized Counts (%)
100
50
0
10¹
10⁴
10⁷
Fluorescence (520 nm)
hSTING R232, HEK293
GFP-Halo, HeLa
GFP-Halo, HEK293T

Figure 20. Constitutive sfCherry reporter

A Constitutive sfCherry reporter line imaged with the Leica Stellaris 8 confocal microscope. **B** Media fluorescence was measured after 2 day culture for both transfected and wild-type cells. **C** Transfected and wild-type cells were analyzed by flow cytometry.

A

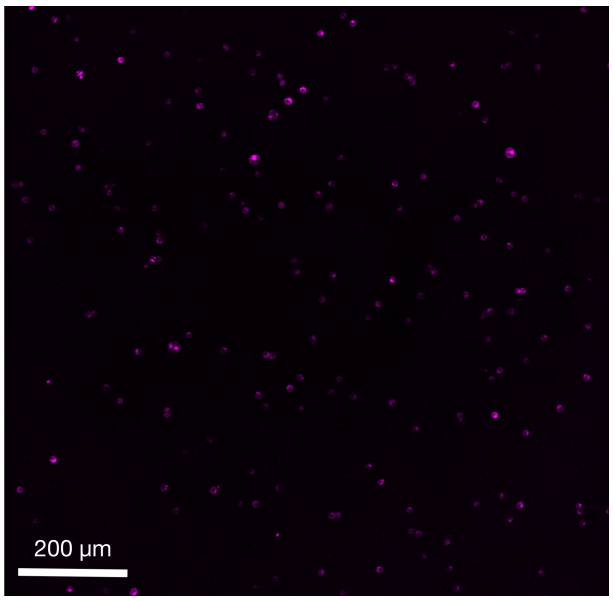
200 µm

B

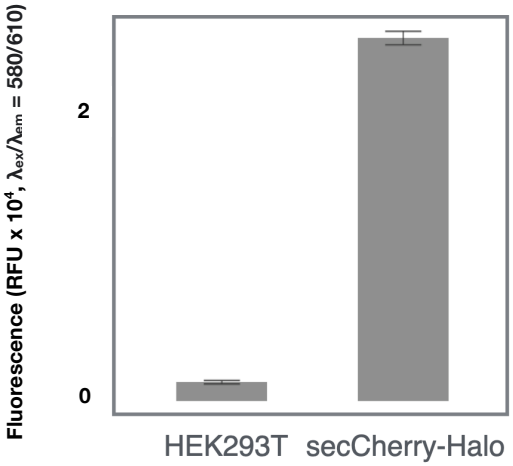
Fluorescence (RFU x 10⁴, λex/λem = 580/610)
2
0
HEK293T
secCherry-Halo

C

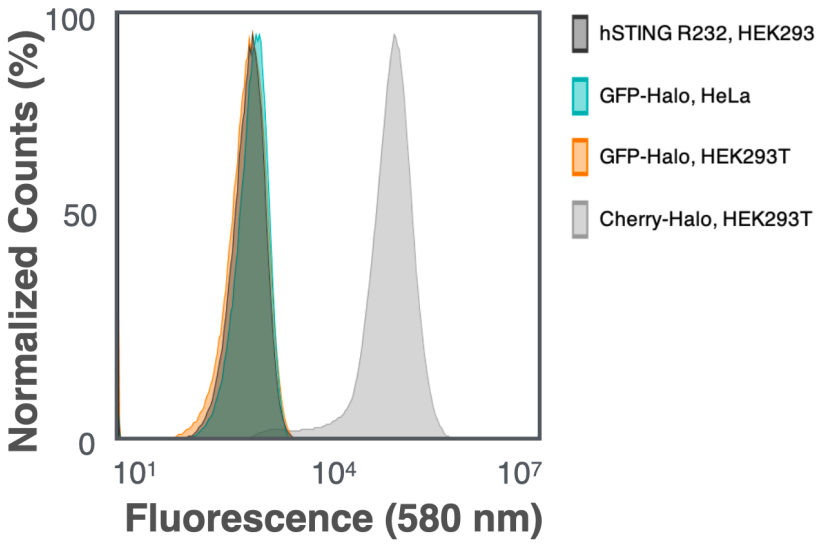
Normalized Counts (%)
100
50
0
10¹
10⁴
10⁷
Fluorescence (580 nm)
hSTING R232, HEK293
GFP-Halo, HeLa
GFP-Halo, HEK293T
Cherry-Halo, HEK293T

HEK293T cell line fluorescence signal was 100-fold higher than wild-type HEK293T cell fluorescence by flow cytometry (**Fig 20B**). The engineered cells lines differed from wild-type in that they were more fluorescent under confocal microscopy and flow cytometry, correlating with media fluorescence measurements.

Multiple analytical approaches collectively substantiated the successful generation of a second color reporter line. Media fluorimetry, flow cytometry, and microscopy data all agreed. The Cherry-Halo cell line was significantly more fluorescent than wild-type cells in all analyses. Furthermore, the red-shifted Cherry fluorescence is potentially advantageous moving forward with cellular assay design. Background media fluorescence and microcarrier bead autofluorescence was generally lower at the Cherry emission wavelength. Like the GFP-Halo line analysis, HaloTag function must still be confirmed.

The importance of having GFP-Halo and Cherry-Halo as dual reporters stems from needing to verify that there is no crosstalk between cells on different microcarriers. Ideally, after compound photorelease from the microcarriers that the cells are grown on, the compound would only stimulate cells that are on the immediate microcarrier and not cells on neighboring microcarriers. Furthermore, once cells secrete reporter protein, it is important that only the microcarrier they are grown on captures the reporter, and not neighboring microcarriers. If substantial signaling is observed on beads that do not display the photocleavable control compound, this would result in false positive “hits” in our DEL compound screen. With these engineered dual reporter cell lines, the stage is set to determine whether cells are only induced by compound released from and secreting reporter that is only captured by

the compound-displaying microcarrier on which they grow.

Conclusion: The Future of Cellular DNA-Encoded Library Screening Platforms

We have laid the groundwork for cellular DEL-based screening. We showed that cells grown on microcarriers were viable qualitatively and quantitatively and produced detectable signal. We found a robust positive control agonist with which novel compound hits will be compared. We demonstrated that UV irradiation at 365 nm was cytotoxic, but photodosing at 385-400 nm was amenable to cell viability and compound photorelease to induce cell signaling. Finally, we engineered a cell reporter whose readout would be more amenable to high-throughput screening. Moving forward, HaloTag function must be confirmed. From there, the constitutively expressing lines will be used to confirm that a secreted, affinity-tagged reporter can be captured on a ligand-functionalizing microcarrier. Finally, inducible lines must be generated to complete proof-of-concept studies. These critical experiments will collectively establish the feasibility of measuring cellular signaling induced by a DEL member and detectable as selective host microcarrier labeling in flow cytometry. In so doing, we will have rendered DEL technology compatible with conventional cellular assays in a format that is highly accessible to most drug discovery groups.

Works Referenced

(1) Shinn, P.; Chen, L.; Ferrer, M.; Itkin, Z.; Klumpp-Thomas, C.; McKnight, C.; Michael, S.; Mierzwa, T.; Thomas, C.; Wilson, K.; Guha, R. High-Throughput Screening for Drug Combinations. In *Bioinformatics and Drug Discovery*; Larson, R. S., Oprea, T. I., Eds.; Springer New York: New York, NY, 2019; pp 11–35. https://doi.org/10.1007/978-1-4939-9089-4_2.

(2) Yasi, E. A.; Kruyer, N. S.; Peralta-Yahya, P. Advances in G Protein-Coupled Receptor High-Throughput Screening. *Curr. Opin. Biotechnol.* **2020**, *64*, 210–217. https://doi.org/10.1016/j.copbio.2020.06.004.

(3) Heine, P.; Witt, G.; Gilardi, A.; Gribbon, P.; Kummer, L.; Plückthun, A. High-Throughput Fluorescence Polarization Assay to Identify Ligands Using Purified G Protein-Coupled Receptor. *SLAS Discov. Adv. Sci. Drug Discov.* **2019**, *24* (9), 915–927. https://doi.org/10.1177/2472555219837344.

(4) Sévin, D. C.; Fuhrer, T.; Zamboni, N.; Sauer, U. Nontargeted in Vitro Metabolomics for High-Throughput Identification of Novel Enzymes in Escherichia Coli. *Nat. Methods* **2017**, *14* (2), 187–194. https://doi.org/10.1038/nmeth.4103.

(5) Tronser, T.; Popova, A. A.; Levkin, P. A. Miniaturized Platform for High-Throughput Screening of Stem Cells. *Curr. Opin. Biotechnol.* **2017**, *46*, 141–149. https://doi.org/10.1016/j.copbio.2017.03.005.

(6) Jeucken, A.; Brouwers, J. High-Throughput Screening of Lipidomic Adaptations in Cultured Cells. *Biomolecules* **2019**, *9* (2), 42. https://doi.org/10.3390/biom9020042.

(7) Li, X.; Feng, H.; Li, Z.; Shi, Y.; Tian, J.; Zhao, C.; Yu, M.; Liu, Z.; Li, H.; Shi, B.; Wang, Q.; Li, L.; Wang, D.; Zhu, L.; Liu, R.; Li, Z. High-Throughput Identification and Screening of Single Microbial Cells by Nanobowl Array. *ACS Appl. Mater. Interfaces* **2019**, *11* (48), 44933–44940. https://doi.org/10.1021/acsami.9b08662.

(8) Brazovskaja, A.; Treutlein, B.; Camp, J. G. High-Throughput Single-Cell Transcriptomics on Organoids. *Curr. Opin. Biotechnol.* **2019**, *55*, 167–171. https://doi.org/10.1016/j.copbio.2018.11.002.

(9) Brandenberg, N.; Hoehnel, S.; Kuttler, F.; Homicsko, K.; Ceroni, C.; Ringel, T.; Gjorevski, N.; Schwank, G.; Coukos, G.; Turcatti, G.; Lutolf, M. P. High-Throughput Automated Organoid Culture via Stem-Cell Aggregation in Microcavity Arrays. *Nat. Biomed. Eng.* **2020**, *4* (9), 863–874. https://doi.org/10.1038/s41551-020-0565-2.

(10) Boehnke, K.; Iversen, P. W.; Schumacher, D.; Lallena, M. J.; Haro, R.; Amat, J.; Haybaeck, J.; Liebs, S.; Lange, M.; Schäfer, R.; Regenbrecht, C. R. A.; Reinhard, C.; Velasco, J. A. Assay Establishment and Validation of a High-Throughput Screening Platform for Three-Dimensional Patient-Derived Colon Cancer Organoid Cultures. *J. Biomol. Screen.* **2016**, *21* (9), 931–941. https://doi.org/10.1177/1087057116650965.

(11) Cochrane, W. G.; Malone, M. L.; Dang, V. Q.; Cavett, V.; Satz, A. L.; Paegel, B. M. Activity-Based DNA-Encoded Library Screening. *ACS Comb. Sci.* **2019**, *21* (5), 425–435. https://doi.org/10.1021/acscombsci.9b00037.

(12) Bassi, G.; Favalli, N.; Vuk, M.; Catalano, M.; Martinelli, A.; Trenner, A.; Porro, A.; Yang, S.; Tham, C. L.; Moroglu, M.; Yue, W. W.; Conway, S. J.; Vogt, P. K.;

Sartori, A. A.; Scheuermann, J.; Neri, D. A Single-Stranded DNA-Encoded Chemical Library Based on a Stereoisomeric Scaffold Enables Ligand Discovery by Modular Assembly of Building Blocks. *Adv. Sci.* **2020**, *7* (22), 2001970. https://doi.org/10.1002/advs.202001970.

(13) Clark, M. A.; Acharya, R. A.; Arico-Muendel, C. C.; Belyanskaya, S. L.; Benjamin, D. R.; Carlson, N. R.; Centrella, P. A.; Chiu, C. H.; Creaser, S. P.; Cuozzo, J. W.; Davie, C. P.; Ding, Y.; Franklin, G. J.; Franzen, K. D.; Gefter, M. L.; Hale, S. P.; Hansen, N. J. V.; Israel, D. I.; Jiang, J.; Kavarana, M. J.; Kelley, M. S.; Kollmann, C. S.; Li, F.; Lind, K.; Mataruse, S.; Medeiros, P. F.; Messer, J. A.; Myers, P.; O'Keefe, H.; Oliff, M. C.; Rise, C. E.; Satz, A. L.; Skinner, S. R.; Svendsen, J. L.; Tang, L.; van Vloten, K.; Wagner, R. W.; Yao, G.; Zhao, B.; Morgan, B. A. Design, Synthesis and Selection of DNA-Encoded Small-Molecule Libraries. *Nat. Chem. Biol.* **2009**, *5* (9), 647–654. https://doi.org/10.1038/nchembio.211.

(14) Harris, P. A.; Berger, S. B.; Jeong, J. U.; Nagilla, R.; Bandyopadhyay, D.; Campobasso, N.; Capriotti, C. A.; Cox, J. A.; Dare, L.; Dong, X.; Eidam, P. M.; Finger, J. N.; Hoffman, S. J.; Kang, J.; Kasparcova, V.; King, B. W.; Lehr, R.; Lan, Y.; Leister, L. K.; Lich, J. D.; MacDonald, T. T.; Miller, N. A.; Ouellette, M. T.; Pao, C. S.; Rahman, A.; Reilly, M. A.; Rendina, A. R.; Rivera, E. J.; Schaeffer, M. C.; Sehon, C. A.; Singhaus, R. R.; Sun, H. H.; Swift, B. A.; Totoritis, R. D.; Vossenkämper, A.; Ward, P.; Wisnoski, D. D.; Zhang, D.; Marquis, R. W.; Gough, P. J.; Bertin, J. Discovery of a First-in-Class Receptor Interacting Protein 1 (RIP1) Kinase Specific Clinical Candidate (GSK2982772) for the Treatment of

Inflammatory Diseases. *J. Med. Chem.* **2017**, *60* (4), 1247–1261. https://doi.org/10.1021/acs.jmedchem.6b01751.

(15) Harris, P. A.; King, B. W.; Bandyopadhyay, D.; Berger, S. B.; Campobasso, N.; Capriotti, C. A.; Cox, J. A.; Dare, L.; Dong, X.; Finger, J. N.; Grady, L. C.; Hoffman, S. J.; Jeong, J. U.; Kang, J.; Kasparcova, V.; Lakdawala, A. S.; Lehr, R.; McNulty, D. E.; Nagilla, R.; Ouellette, M. T.; Pao, C. S.; Rendina, A. R.; Schaeffer, M. C.; Summerfield, J. D.; Swift, B. A.; Totoritis, R. D.; Ward, P.; Zhang, A.; Zhang, D.; Marquis, R. W.; Bertin, J.; Gough, P. J. DNA-Encoded Library Screening Identifies Benzo[*b*][1,4]Oxazepin-4-Ones as Highly Potent and Monoselective Receptor Interacting Protein 1 Kinase Inhibitors. *J. Med. Chem.* **2016**, *59* (5), 2163–2178. https://doi.org/10.1021/acs.jmedchem.5b01898.

(16) Yang, H.; Medeiros, P. F.; Raha, K.; Elkins, P.; Lind, K. E.; Lehr, R.; Adams, N. D.; Burgess, J. L.; Schmidt, S. J.; Knight, S. D.; Auger, K. R.; Schaber, M. D.; Franklin, G. J.; Ding, Y.; DeLorey, J. L.; Centrella, P. A.; Mataruse, S.; Skinner, S. R.; Clark, M. A.; Cuozzo, J. W.; Evindar, G. Discovery of a Potent Class of PI3Kα Inhibitors with Unique Binding Mode via Encoded Library Technology (ELT). *ACS Med. Chem. Lett.* **2015**, *6* (5), 531–536. https://doi.org/10.1021/acsmedchemlett.5b00025.

(17) Chan, A. I.; McGregor, L. M.; Jain, T.; Liu, D. R. Discovery of a Covalent Kinase Inhibitor from a DNA-Encoded Small-Molecule Library × Protein Library Selection. *J. Am. Chem. Soc.* **2017**, *139* (30), 10192–10195. https://doi.org/10.1021/jacs.7b04880.

(18) Dawadi, S.; Simmons, N.; Miklossy, G.; Bohren, K. M.; Faver, J. C.; Ucisik, M. N.; Nyshadham, P.; Yu, Z.; Matzuk, M. M. Discovery of Potent Thrombin Inhibitors from a Protease-Focused DNA-Encoded Chemical Library. *Proc. Natl. Acad. Sci.* **2020**, *117* (29), 16782–16789. https://doi.org/10.1073/pnas.2005447117.

(19) Ding, Y.; Belyanskaya, S.; DeLorey, J. L.; Messer, J. A.; Joseph Franklin, G.; Centrella, P. A.; Morgan, B. A.; Clark, M. A.; Skinner, S. R.; Dodson, J. W.; Li, P.; Marino, J. P.; Israel, D. I. Discovery of Soluble Epoxide Hydrolase Inhibitors through DNA-Encoded Library Technology (ELT). *Bioorg. Med. Chem.* **2021**, *41*, 116216. https://doi.org/10.1016/j.bmc.2021.116216.

(20) Deng, H.; Zhou, J.; Sundersingh, F.; Messer, J. A.; Somers, D. O.; Ajakane, M.; Arico-Muendel, C. C.; Beljean, A.; Belyanskaya, S. L.; Bingham, R.; Blazensky, E.; Boullay, A.-B.; Boursier, E.; Chai, J.; Carter, P.; Chung, C.-W.; Daugan, A.; Ding, Y.; Herry, K.; Hobbs, C.; Humphries, E.; Kollmann, C.; Nguyen, V. L.; Nicodeme, E.; Smith, S. E.; Dodic, N.; Ancellin, N. Discovery and Optimization of Potent, Selective, and *in Vivo* Efficacious 2-Aryl Benzimidazole BCATm Inhibitors. *ACS Med. Chem. Lett.* **2016**, *7* (4), 379–384. https://doi.org/10.1021/acsmedchemlett.5b00389.

(21) Wu, Z.; Graybill, T. L.; Zeng, X.; Platchek, M.; Zhang, J.; Bodmer, V. Q.; Wisnoski, D. D.; Deng, J.; Coppo, F. T.; Yao, G.; Tamburino, A.; Scavello, G.; Franklin, G. J.; Mataruse, S.; Bedard, K. L.; Ding, Y.; Chai, J.; Summerfield, J.; Centrella, P. A.; Messer, J. A.; Pope, A. J.; Israel, D. I. Cell-Based Selection Expands the Utility of DNA-Encoded Small-Molecule Library Technology to Cell Surface Drug Targets:

Identification of Novel Antagonists of the NK3 Tachykinin Receptor. *ACS Comb. Sci.* **2015**, *17* (12), 722–731. https://doi.org/10.1021/acscombsci.5b00124.

(22) Xie, J.; Wang, S.; Ma, P.; Ma, F.; Li, J.; Wang, W.; Lu, F.; Xiong, H.; Gu, Y.; Zhang, S.; Xu, H.; Yang, G.; Lerner, R. A. Selection of Small Molecules That Bind to and Activate the Insulin Receptor from a DNA-Encoded Library of Natural Products. *iScience* **2020**, *23* (6), 101197. https://doi.org/10.1016/j.isci.2020.101197.

(23) Huang, Y.; Meng, L.; Nie, Q.; Zhou, Y.; Chen, L.; Yang, S.; Fung, Y. M. E.; Li, X.; Huang, C.; Cao, Y.; Li, Y.; Li, X. Selection of DNA-Encoded Chemical Libraries against Endogenous Membrane Proteins on Live Cells. *Nat. Chem.* **2021**, *13* (1), 77–88. https://doi.org/10.1038/s41557-020-00605-x.

(24) Ahn, S.; Kahsai, A. W.; Pani, B.; Wang, Q.-T.; Zhao, S.; Wall, A. L.; Strachan, R. T.; Staus, D. P.; Wingler, L. M.; Sun, L. D.; Sinnaeve, J.; Choi, M.; Cho, T.; Xu, T. T.; Hansen, G. M.; Burnett, M. B.; Lamerdin, J. E.; Bassoni, D. L.; Gavino, B. J.; Husemoen, G.; Olsen, E. K.; Franch, T.; Costanzi, S.; Chen, X.; Lefkowitz, R. J. Allosteric “Beta-Blocker” Isolated from a DNA-Encoded Small Molecule Library. *Proc. Natl. Acad. Sci.* **2017**, *114* (7), 1708–1713. https://doi.org/10.1073/pnas.1620645114.

(25) Brown, D. G.; Brown, G. A.; Centrella, P.; Certel, K.; Cooke, R. M.; Cuozzo, J. W.; Dekker, N.; Dumelin, C. E.; Ferguson, A.; Fiez-Vandal, C.; Geschwindner, S.; Guié, M.-A.; Habeshian, S.; Keefe, A. D.; Schlenker, O.; Sigel, E. A.; Snijder, A.; Soutter, H. T.; Sundström, L.; Troast, D. M.; Wiggin, G.; Zhang, J.; Zhang, Y.; Clark, M. A. Agonists and Antagonists of Protease-Activated Receptor 2 Discovered within a DNA-Encoded Chemical Library Using Mutational Stabilization of the Target.

SLAS Discov. Adv. Sci. Drug Discov. **2018**, *23* (5), 429–436. https://doi.org/10.1177/2472555217749847.

(26) Kunig, V. B. K.; Potowski, M.; Klika Škopić, M.; Brunschweiger, A. Scanning Protein Surfaces with DNA-Encoded Libraries. *ChemMedChem* **2021**, *16* (7), 1048–1062. https://doi.org/10.1002/cmdc.202000869.

(27) Kunig, V. B. K.; Potowski, M.; Akbarzadeh, M.; Klika Škopić, M.; Santos Smith, D.; Arendt, L.; Dormuth, I.; Adihou, H.; Andlovic, B.; Karatas, H.; Shaabani, S.; Zarganes-Tzitzikas, T.; Neochoritis, C. G.; Zhang, R.; Groves, M.; Guéret, S. M.; Ottmann, C.; Rahnenführer, J.; Fried, R.; Dömling, A.; Brunschweiger, A. TEAD–YAP Interaction Inhibitors and MDM2 Binders from DNA-Encoded Indole-Focused Ugi Peptidomimetics. *Angew. Chem. Int. Ed.* **2020**, *59* (46), 20338–20342. https://doi.org/10.1002/anie.202006280.

(28) Kollmann, C. S.; Bai, X.; Tsai, C.-H.; Yang, H.; Lind, K. E.; Skinner, S. R.; Zhu, Z.; Israel, D. I.; Cuozzo, J. W.; Morgan, B. A.; Yuki, K.; Xie, C.; Springer, T. A.; Shimaoka, M.; Evindar, G. Application of Encoded Library Technology (ELT) to a Protein–Protein Interaction Target: Discovery of a Potent Class of Integrin Lymphocyte Function-Associated Antigen 1 (LFA-1) Antagonists. *Bioorg. Med. Chem.* **2014**, *22* (7), 2353–2365. https://doi.org/10.1016/j.bmc.2014.01.050.

(29) Heinis, C.; Winter, G. Encoded Libraries of Chemically Modified Peptides. *Curr. Opin. Chem. Biol.* **2015**, *26*, 89–98. https://doi.org/10.1016/j.cbpa.2015.02.008.

(30) Barriscale, K. A.; O'Sullivan, S. A.; McCarthy, T. V. A Single Secreted Luciferase-Based Gene Reporter Assay. *Anal. Biochem.* **2014**, *453*, 44–49. https://doi.org/10.1016/j.ab.2014.02.019.

(31) Kandarian, F.; Sunga, G. M.; Arango-Saenz, D.; Rossetti, M. A Flow Cytometry-Based Cytotoxicity Assay for the Assessment of Human NK Cell Activity. *J. Vis. Exp.* **2017**, No. 126, 56191. https://doi.org/10.3791/56191.

(32) Chang, Q.; Ornatsky, O. I.; Siddiqui, I.; Loboda, A.; Baranov, V. I.; Hedley, D. W. Imaging Mass Cytometry. *Cytometry A* **2017**, *91* (2), 160–169. https://doi.org/10.1002/cyto.a.23053.

(33) Chen, Q.; Sun, L.; Chen, Z. J. Regulation and Function of the CGAS–STING Pathway of Cytosolic DNA Sensing. *Nat. Immunol.* **2016**, *17* (10), 1142–1149. https://doi.org/10.1038/ni.3558.

(34) Kwon, J.; Bakhoum, S. F. The Cytosolic DNA-Sensing CGAS–STING Pathway in Cancer. *Cancer Discov.* **2020**, *10* (1), 26–39. https://doi.org/10.1158/2159-8290.CD-19-0761.

(35) Li, Q.; Wang, Q.; Wang, O.; Shao, K.; Lin, H.; Lei, Y. A Simple and Scalable Hydrogel-Based System for Culturing Protein-Producing Cells. *PLOS ONE* **2018**, *13* (1), e0190364. https://doi.org/10.1371/journal.pone.0190364.

(36) Langer, K.; Joensson, H. N. Rapid Production and Recovery of Cell Spheroids by Automated Droplet Microfluidics. *SLAS Technol. Transl. Life Sci. Innov.* **2020**, *25* (2), 111–122. https://doi.org/10.1177/2472630319877376.

(37) Weber, T. S.; Jaehnert, I.; Schichor, C.; Or-Guil, M.; Carneiro, J. Quantifying the Length and Variance of the Eukaryotic Cell Cycle Phases by a Stochastic Model and Dual Nucleoside Pulse Labelling. *PLoS Comput. Biol.* **2014**, *10* (7), e1003616. https://doi.org/10.1371/journal.pcbi.1003616.

(38) Derakhti, S.; Safiabadi-Tali, S. H.; Amoabediny, G.; Sheikhpour, M. Attachment and Detachment Strategies in Microcarrier-Based Cell Culture Technology: A Comprehensive Review. *Mater. Sci. Eng. C* **2019**, *103*, 109782. https://doi.org/10.1016/j.msec.2019.109782.

(39) Huang, L.; Abdalla, A. M. E.; Xiao, L.; Yang, G. Biopolymer-Based Microcarriers for Three-Dimensional Cell Culture and Engineered Tissue Formation. *Int. J. Mol. Sci.* **2020**, *21* (5), 1895. https://doi.org/10.3390/ijms21051895.

(40) Decherchi, P.; Cochard, P.; Gauthier, P. Dual Staining Assessment of Schwann Cell Viability within Whole Peripheral Nerves Using Calcein-AM and Ethidium Homodimer. *J. Neurosci. Methods* **1997**, *71* (2), 205–213. https://doi.org/10.1016/S0165-0270(96)00146-X.

(41) Bakos, É.; Német, O.; Patik, I.; Kucsma, N.; Várady, G.; Szakács, G.; Özvegy-Laczka, C. A Novel Fluorescence-based Functional Assay for Human OATP1A2 and OATP1C1 Identifies Interaction between Third-generation P-gp Inhibitors and OATP1A2. *FEBS J.* **2020**, *287* (12), 2468–2485. https://doi.org/10.1111/febs.15156.

(42) Gao, P.; Ascano, M.; Zillinger, T.; Wang, W.; Dai, P.; Serganov, A. A.; Gaffney, B. L.; Shuman, S.; Jones, R. A.; Deng, L.; Hartmann, G.; Barchet, W.; Tuschl, T.; Patel, D. J. Structure-Function Analysis of STING Activation by

c[G(2′,5′)PA(3′,5′)p] and Targeting by Antiviral DMXAA. *Cell* **2013**, *154* (4), 748–762. https://doi.org/10.1016/j.cell.2013.07.023.

(43) Ding, C.; Song, Z.; Shen, A.; Chen, T.; Zhang, A. Small Molecules Targeting the Innate Immune CGAS-STING-TBK1 Signaling Pathway. *Acta Pharm. Sin. B* **2020**, *10* (12), 2272–2298. https://doi.org/10.1016/j.apsb.2020.03.001.

(44) Chin, E. N.; Yu, C.; Vartabedian, V. F.; Jia, Y.; Kumar, M.; Gamo, A. M.; Vernier, W.; Ali, S. H.; Kissai, M.; Lazar, D. C.; Nguyen, N.; Pereira, L. E.; Benish, B.; Woods, A. K.; Joseph, S. B.; Chu, A.; Johnson, K. A.; Sander, P. N.; Martínez-Peña, F.; Hampton, E. N.; Young, T. S.; Wolan, D. W.; Chatterjee, A. K.; Schultz, P. G.; Petrassi, H. M.; Teijaro, J. R.; Lairson, L. L. Antitumor Activity of a Systemic STING-Activating Non-Nucleotide CGAMP Mimetic. *Science* **2020**, *369* (6506), 993–999. https://doi.org/10.1126/science.abb4255.

(45) Yi, G.; Brendel, V. P.; Shu, C.; Li, P.; Palanathan, S.; Cheng Kao, C. Single Nucleotide Polymorphisms of Human STING Can Affect Innate Immune Response to Cyclic Dinucleotides. *PLoS ONE* **2013**, *8* (10), e77846. https://doi.org/10.1371/journal.pone.0077846.

(46) Pan, B.-S.; Perera, S. A.; Piesvaux, J. A.; Presland, J. P.; Schroeder, G. K.; Cumming, J. N.; Trotter, B. W.; Altman, M. D.; Buevich, A. V.; Cash, B.; Cemerski, S.; Chang, W.; Chen, Y.; Dandliker, P. J.; Feng, G.; Haidle, A.; Henderson, T.; Jewell, J.; Kariv, I.; Knemeyer, I.; Kopinja, J.; Lacey, B. M.; Laskey, J.; Lesburg, C. A.; Liang, R.; Long, B. J.; Lu, M.; Ma, Y.; Minnihan, E. C.; O'Donnell, G.; Otte, R.; Price, L.; Rakhilina, L.; Sauvagnat, B.; Sharma, S.; Tyagarajan, S.; Woo, H.; Wyss, D. F.; Xu, S.; Bennett, D. J.; Addona, G. H. An Orally Available Non-Nucleotide

STING Agonist with Antitumor Activity. *Science* **2020**, *369* (6506), eaba6098. https://doi.org/10.1126/science.aba6098.

(47) Wong, D. Y.; Ranganath, T.; Kasko, A. M. Low-Dose, Long-Wave UV Light Does Not Affect Gene Expression of Human Mesenchymal Stem Cells. *PLOS ONE* **2015**, *10* (9), e0139307. https://doi.org/10.1371/journal.pone.0139307.

(48) Garbujo, S.; Galbiati, E.; Salvioni, L.; Mazzucchelli, M.; Frascotti, G.; Sun, X.; Megahed, S.; Feliu, N.; Prosperi, D.; Parak, W. J.; Colombo, M. Functionalization of Colloidal Nanoparticles with a Discrete Number of Ligands Based on a "HALO-Bioclick" Reaction. *Chem. Commun.* **2020**, *56* (77), 11398–11401. https://doi.org/10.1039/D0CC04355A.

(49) Qin, J. Y.; Zhang, L.; Clift, K. L.; Hulur, I.; Xiang, A. P.; Ren, B.-Z.; Lahn, B. T. Systematic Comparison of Constitutive Promoters and the Doxycycline-Inducible Promoter. *PLoS ONE* **2010**, *5* (5), e10611. https://doi.org/10.1371/journal.pone.0010611.

(50) Cong, L.; Ran, F. A.; Cox, D.; Lin, S.; Barretto, R.; Habib, N.; Hsu, P. D.; Wu, X.; Jiang, W.; Marraffini, L. A.; Zhang, F. Multiplex Genome Engineering Using CRISPR/Cas Systems. *Science* **2013**, *339* (6121), 819–823. https://doi.org/10.1126/science.1231143.

(51) Mali, P.; Yang, L.; Esvelt, K. M.; Aach, J.; Guell, M.; DiCarlo, J. E.; Norville, J. E.; Church, G. M. RNA-Guided Human Genome Engineering via Cas9. *Science* **2013**, *339* (6121), 823–826. https://doi.org/10.1126/science.1232033.